

# Data-Driven Matrix Recovery with High-Dimensional Noise via Optimal Shrinkage of Singular Values and Wavelet Shrinkage of Singular Vectors

Pei-Chun Su

*Department of Applied Mathematics, Yale University, USA*

July 15, 2025

## Abstract

This paper presents a novel data-driven algorithm designed to recover low-rank matrices whose entries satisfy a mixed Hölder condition in the presence of high-dimensional noise with a separable covariance structure. The algorithm, coined *extended optimal shrinkage and wavelet shrinkage* (eOWS), emphasizes the asymptotic structure, where the matrix size is significantly larger than the rank of the signal matrix. The denoising process begins with the adaptation of the well-known optimal shrinkage of singular values. This is followed by an iterative procedure that organizes the matrix using a coupled metric on the rows and columns, constructed by building a tree structure for both dimensions. This hierarchical organization induces a tensor Haar-Walsh basis on the matrix. An adapted wavelet shrinkage technique is applied to further denoise the reconstructed matrix, modifying the Haar-Walsh coefficients based on the analysis of the first-order perturbation of singular vectors. We provide theoretical guarantees for these estimators, demonstrating a convergence rate that highlights the efficacy of our algorithm. Simulations show successful matrix recovery, with a small mean squared error between the estimate and the ground truth, and accurate reconstruction of the singular vector spaces.

# 1 Introduction

We aim to denoise a  $p \times n$  data matrix  $\tilde{S}(x, y)$ , comprised of  $n \in \mathbb{N}$  noisy samples of dimension  $p \in \mathbb{N}$ . The data matrix is modeled as follows.

$$\tilde{S} = S + Z \in \mathbb{R}^{p \times n}. \quad (1)$$

$Z(x, y)$  is a noise-only random matrix, potentially with a dependence structure that will be detailed later.  $S(x, y)$  is the signal matrix satisfying a mixed Hölder condition that will be defined later, and is a low-rank matrix with the singular value decomposition (SVD)  $\sum_{i=1}^r d_i \mathbf{u}_i \mathbf{v}_i^\top$ , where  $r \geq 1$  is assumed to be small compared with  $p$  and  $n$ ,  $\mathbf{u}_i \in \mathbb{R}^p$  and  $\mathbf{v}_i \in \mathbb{R}^n$  are left and right singular vectors, respectively, prescribing the signal, and  $d_i > 0$  are the associated singular values describing signal strength that may depend on  $n$ . To simplify the discussion, we call the pair  $\mathbf{u}_i$  and  $\mathbf{v}_i$  the  $i$ -th signal and  $d_i$  the  $i$ -th signal strength hereafter. The *high dimensional* setup under the model (1) is  $p = p(n)$  and  $p/n \rightarrow \beta \in (0, \infty)$  as  $n \rightarrow \infty$ . This model is a generalization of the traditional high-dimensional spiked model [6, 7, 8]. We review two shrinkage-based approaches for recovering the underlying matrix  $S$  in the following. The first is designed for low-rank structures, leveraging spectral decay to recover dominant singular components; the second is designed for the mixed Hölder condition, utilizing localized basis shrinkage to capture piecewise smooth features.

## 1.1 Optimal Shrinkage of Singular Values

When  $S$  is low-rank, a weighting approach has been actively studied to recover  $S$  from  $\tilde{S}$  by SVD, widely known in the literature as the singular value shrinkage, for recovering  $S$ , which was first mentioned, to the best of our knowledge, in [23, 37, 28]. The idea is to select a proper function  $\varphi : [0, \infty) \rightarrow [0, \infty)$ , often nonlinear, and construct

$$\hat{S}_\varphi = \sum_{i=1}^{p \wedge n} \varphi(\tilde{\lambda}_i) \tilde{\mathbf{u}}_i \tilde{\mathbf{v}}_i^\top \quad (2)$$

as an estimate of  $S$ , where  $\tilde{\lambda}_1 \geq \tilde{\lambda}_2 \geq \dots \geq \tilde{\lambda}_{p \wedge n} \geq 0$  are common eigenvalues of  $\tilde{S}\tilde{S}^\top$  and  $\tilde{S}^\top\tilde{S}$  and  $\{\tilde{\mathbf{u}}_i\}_{i=1}^p$  and  $\{\tilde{\mathbf{v}}_i\}_{i=1}^n$  are the left and right singular vectors of  $\tilde{S}$  respectively.  $\varphi$  is termed as a shrinker. By employing a loss function  $L_n : \mathbb{R}^{p \times n} \times \mathbb{R}^{p \times n} \rightarrow \mathbb{R}_+$  to quantify the discrepancy between  $\hat{S}_\varphi$  and  $S$ , the associated *optimal shrinker*, if it exists, is defined as  $\varphi^* :=$

$\arg \min_{\varphi} \lim_{n \rightarrow \infty} L_n(\hat{S}_{\varphi}, S)$ . Common loss functions include the Frobenius norm and operator norm of  $\hat{S}_{\varphi} - S$ . This approach is termed as *Optimal Shrinkage* ( $\mathcal{OS}$ ) in previous literatures [18, 26]. Under the spiked model, many works [38, 26, 40, 32, 33, 30, 19, 44] investigate this matrix denoising problem and develop the associated  $\mathcal{OS}$  with various assumptions on the noise matrix  $Z$ .

In [44], we considered a special case, the separable covariance structure

$$Z = \mathcal{A}^{1/2} \mathcal{X} \mathcal{B}^{1/2}, \quad (3)$$

where  $\mathcal{X}$  is a random matrix with independent entries and some moment conditions, and  $\mathcal{A}$  and  $\mathcal{B}$  are respectively  $p \times p$  and  $n \times n$  deterministic positive-definite matrices that describe the color and dependence structure of noise, respectively. We extended the results in [9, 10] and derived an fully data-driven algorithm *eOptShrink* to estimate effective rank and the spectral density distribution of  $Z$ , and thus a precise estimate the amount of bias in singular values and singular vectors, and optimal shrinkers, compared to existing approaches [26, 19, 38].

The approach of  $\mathcal{OS}$  and *eOptShrink* has found wide applications, such as diffusion magnetic resonance imaging denoising [46], fetal electrocardiogram (fECG) extraction from the trans-abdominal maternal ECG (tamECG) [42, 44], ECG T-wave quality evaluation [43], enhancing 3-D seismic data [5], otoacoustic emission signal denoising [36], stimulation artifact removal from intracranial electroencephalogram (EEG) [1], and cardiogenic artifact removal from EEG [13], among many others.

Optimal shrinkage-related methods, while effective through the modification of singular values as in (2), do not fully account for the errors induced by the biased singular vectors  $\tilde{\mathbf{u}}_i$  and  $\tilde{\mathbf{v}}_i$ . This perturbation is especially significant in high-dimensional settings, leading to a degradation in the quality of the estimated signal matrix, even if the singular values are optimally shrunk. For example, consider the dimension reduction approach using SVD. This bias distorts the signal representation, resulting in suboptimal performance in downstream tasks such as classification and clustering. Therefore, while optimal shrinkage can effectively recover the data matrix by modifying singular values, it is crucial to consider methods that also address the correction of singular vectors.

## 1.2 Mixed Hölder Matrix Recovery via Wavelet Shrinkage

Denote the row space and column space of  $S$  by  $X = \{x_1, \dots, x_p\}$  and  $Y = \{y_1, \dots, y_n\}$ , where  $x_i$  for  $i = 1, \dots, p$  is the  $i$ -th row of  $S$  and  $y_j$  for

$j = 1, \dots, n$  is the  $j$ -th column of  $S$ . Furthermore, we define

$$S(x_i, y_j) := S_{ij} \quad (4)$$

as the  $ij$ -th entry of  $S$ . Assume  $X$  and  $Y$  are equipped with a pair of partition tree and tree metric  $(T_X, d_X)$  and  $(T_Y, d_Y)$  respectively, a *mixed Hölder* condition of  $S$  can be defined as (20). The mixed Hölder condition characterizes the mixed variation of  $S$  [2]. Besides, tree structures  $T_X$  and  $T_Y$  characterize a classical Haar basis on  $X$  and  $Y$  [14, 25, 27]. Given Haar systems  $\{\omega_I\}$  on  $X$  and  $\{\omega_J\}$  on  $Y$ , we can consider their tensor product; this is the collection of all functions

$$\Phi_{IJ}(x, y) = \omega_I(x)\omega_J(y). \quad (5)$$

These functions form an orthonormal basis for the collection of all functions with mean zero on  $X \times Y$ . Define the discrete wavelet coefficient of  $S$  on the basis  $\Phi_{IJ}$  as

$$\langle S, \Phi_{IJ} \rangle := \sum_{x \in I, y \in J} S(x, y) \Phi_{IJ}(x, y). \quad (6)$$

Then  $S$  can be expanded by the wavelet transform as

$$S(x, y) = \sum_{\Phi_{IJ}} \langle S, \Phi_{IJ} \rangle \Phi_{IJ}(x, y). \quad (7)$$

When  $S$  is a mixed Hölder matrix with norm  $L$ , contaminated by additive noise  $Z$  according to the model (1), the *Wavelet Shrinkage* ( $\mathcal{WS}$ ) scheme by Donoho and Johnstone [20, 21, 22] is applied, to construct an estimator from the noisy observation  $\tilde{S}$ . Specifically, the matrix  $\tilde{S}$  is expanded in a two-dimensional Haar wavelet series:

$$\tilde{S}(x, y) = \sum_{\Phi_{IJ}} \langle \tilde{S}, \Phi_{IJ} \rangle \Phi_{IJ}(x, y). \quad (8)$$

When the entries of  $Z$  are assumed to be i.i.d. and normally distributed with mean 0 and variance  $\sigma^2$ , each observed wavelet coefficient  $\langle \tilde{S}, \Phi_{IJ} \rangle$  follows a normal distribution centered at the true coefficient  $\langle S, \Phi_{IJ} \rangle$ . The modified wavelet coefficients are acquired by applying a nonlinear shrinker

$$\eta_t(x) := (|x| - t)_+ \operatorname{sgn}(x) \quad (9)$$

to the wavelet coefficients  $\langle \tilde{S}, \Phi_{IJ} \rangle$ , for a threshold value  $t > 0$ . The resulting estimator is  $\hat{C}_{\Phi_{IJ}} = \eta_t(\langle \tilde{S}, \Phi_{IJ} \rangle)$ , and the resulting estimate of the matrix  $S$  is

$$\hat{S}_{\eta_t}(x, y) = \sum_{\Phi_{IJ}} \hat{C}_{\Phi_{IJ}} \Phi_{IJ}(x, y). \quad (10)$$

Further details of finding the optimal shrinker  $\eta_t^*$  and its theoretical guarantees will be reviewed in Section 2.3.

However, in practice, the entries of the noise matrix  $Z$  are typically not i.i.d normally distributed (model in (3) for example). Additionally, the tree structures  $T_X$  and  $T_Y$  are often derived directly from the raw data matrix (check Appendix B). When the noise  $Z$  is sufficiently strong, it disrupts the tree structure and, consequently, the constructed Haar basis.

### 1.3 Contributions

In this paper, we propose an enhanced method for recovering the signal  $S$ , which is assumed to be low-rank and to satisfy a mixed Hölder condition and is contaminated by the noise with the separable covariance model described in (3). Our method improves existing approaches such as  $\mathcal{OS}$  and  $\mathcal{WS}$  and is coined *extended optimal shrinkage and wavelet shrinkage* ( $\text{eOWS}$ ). The key innovation lies in constructing improved hierarchical trees in the row and column domains of  $\hat{S}_\varphi$ , which produce an improved tree-induced metric and allow the recovery of singular vectors left and right of  $\tilde{\mathbf{u}}_i$  and  $\tilde{\mathbf{v}}_i$  in (2) by  $\mathcal{WS}$ . Moreover, instead of using only the standard Haar basis, we employ the general Haar-Walsh transform (GHWT) [29] combined with a best-basis selection algorithm (eGHWT) [39]. In [41], we demonstrated that eGHWT exhibits improved spectral decay for families of smooth and oscillatory orthogonal polynomials. This leads to better coefficient concentration and more effective denoising. The performance of an estimator  $\hat{S}$  for the ground truth matrix  $S$  is evaluated using the mean squared error (MSE) loss

$$\|\hat{S} - S\|_{2,n}^2 := \frac{\mathcal{L}_n^{\text{fro}}(\hat{S}, S)}{pn}, \quad (11)$$

where  $\mathcal{L}_n^{\text{fro}}(\hat{S}, S) := \|\hat{S} - S\|_F^2 = \sum_{i,j} (\hat{S}_{ij} - S_{ij})^2$  is the Frobenius loss.

Specifically speaking, in  $\text{eOWS}$ , we first construct an estimator  $\hat{S}_{\hat{\varphi}_e}$  from  $\text{eOptShrink}$  with the shrinker.

$$\hat{\varphi}_e(\tilde{\lambda}_i) = \begin{cases} \hat{d}_{e,i} / \sqrt{\hat{a}_{e,1,i} \hat{a}_{e,2,i}}, & \text{if } i = 1, \dots, \hat{r}^+ \\ 0, & \text{otherwise} \end{cases} \quad (12)$$

such that  $\hat{S}_{\hat{\varphi}_e} = \sum_{i=1}^{\hat{r}^+} \hat{\varphi}_e(\tilde{\lambda}_i) \tilde{\mathbf{u}}_i \tilde{\mathbf{v}}_i$ , where  $\hat{r}^+$  is the estimator of an effective rank,  $\hat{d}_{e,i}$  is an estimator of the singular value  $d_i$ ,  $\hat{a}_{e,1,i}$  is an estimator of the inner product of the left singular vectors  $a_{1,i} := \langle \tilde{\mathbf{u}}_i, \mathbf{u}_i \rangle^2$ , and  $\hat{a}_{e,2,i}$  is an estimator of the inner product of right singular vectors  $a_{2,i} := \langle \tilde{\mathbf{v}}_i, \mathbf{v}_i \rangle^2$ . The above estimators are defined in (38), which are precise estimators when  $n$  is sufficiently large [44]. If we assume  $\langle \tilde{\mathbf{u}}_i, \mathbf{u}_i \rangle > 0$  and  $\langle \tilde{\mathbf{v}}_i, \mathbf{v}_i \rangle > 0$  and write the biased singular vectors as  $\tilde{\mathbf{u}}_i = \sqrt{a_{1,i}} \mathbf{u}_i + \Delta \mathbf{u}_i$  and  $\tilde{\mathbf{v}}_i = \sqrt{a_{2,i}} \mathbf{v}_i + \Delta \mathbf{v}_i$ , such that  $\mathbf{u}_i \perp \Delta \mathbf{u}_i$  and  $\mathbf{v}_i \perp \Delta \mathbf{v}_i$ , while comparing  $\hat{S}_{\hat{\varphi}_e}$  with the first  $r^+$  signals from the original data matrix  $S$ , the difference between  $\hat{S}_{\hat{\varphi}_e}$  and  $S_{r^+} = \sum_{i=1}^{r^+} d_i \mathbf{u}_i \mathbf{v}_i^\top$  is

$$\begin{aligned} \hat{S}_{\hat{\varphi}_e} - S_{r^+} &= \hat{S}_{\hat{\varphi}_e} - \sum_{i=1}^{r^+} d_i \mathbf{u}_i \mathbf{v}_i^\top \simeq \sum_{i=1}^{r^+} d_i (\tilde{\mathbf{u}}_i \tilde{\mathbf{v}}_i^\top / \sqrt{a_{1,i} a_{2,i}} - \mathbf{u}_i \mathbf{v}_i^\top) \\ &= \sum_{i=1}^{r^+} d_i (\mathbf{u}_i \Delta \mathbf{v}_i^\top / \sqrt{a_{2,i}} + \Delta \mathbf{u}_i \mathbf{v}_i^\top / \sqrt{a_{1,i}} + \Delta \mathbf{u}_i \Delta \mathbf{v}_i^\top / \sqrt{a_{1,i} a_{2,i}}) \end{aligned} \quad (13)$$

To remove this error, we propose an extended  $\mathcal{WS}$  approach. We construct tree structures  $\mathcal{T}_X$  and  $\mathcal{T}_Y$  in rows and columns in  $S$  applying the Questionnaire [4, 14] approach, which iterates between organizing the rows and columns of the matrix to refine the organization of the other based on a metric related to the Earth Mover's Distance (check Appendix B.2 for details). The coefficients of eGHWT and a best basis  $\{\Phi_{(\mathbf{p}, \mathbf{q})}\}_{(\mathbf{p}, \mathbf{q}) \in \mathcal{B}^*}$  for  $\hat{S}_{\hat{\varphi}_e}$  are thereby induced, where  $\mathcal{B}^*$  is the best tiling of the 4D time sequence domain for  $X \times Y$ ,  $(\mathbf{p}, \mathbf{q})$  corresponds to an area one tile in the best tiling  $\mathcal{B}^*$ , and  $\Phi_{(\mathbf{p}, \mathbf{q})}(x, y) = \omega_{\mathbf{p}}(x) \omega_{\mathbf{q}}(y)$  denotes the tensor Haar-Walsh basis function (see Appendix C for details). Building on the framework introduced in [35], we analyze the first-order perturbation of singular vectors in a high-dimensional context and derive the optimal shrinker  $\eta_{\Phi_{(\mathbf{p}, \mathbf{q})}}^*$  across all of the basis functions induced by the constructed trees, which adapts to different noise models  $Z$ . The denoised estimator is thus constructed as

$$\hat{S}_{\hat{\varphi}_e^*} := \sum_{(\mathbf{p}, \mathbf{q}) \in \mathcal{B}^*} \eta_{\Phi_{(\mathbf{p}, \mathbf{q})}}^* \left( \left\langle \hat{S}_{\hat{\varphi}_e}, \Phi_{(\mathbf{p}, \mathbf{q})} \right\rangle \right) \Phi_{(\mathbf{p}, \mathbf{q})}. \quad (14)$$

Define  $\hat{U}_{\hat{\varphi}_e^*} \in \mathbb{R}^{p \times \hat{r}^+}$  and  $\hat{V}_{\hat{\varphi}_e^*} \in \mathbb{R}^{n \times \hat{r}^+}$  as matrices consisting of the first  $\hat{r}^+$  left and right singular vectors of  $\hat{S}_{\hat{\varphi}_e^*}$ , respectively. These vectors serve as further denoised versions of  $\tilde{U}$  and  $\tilde{V}$ , obtained via the extended  $\mathcal{WS}$

procedure. Let  $\widehat{D}_{\widehat{\varphi}_e^*} = \text{diag}(\widehat{d}_{e,1}, \dots, \widehat{d}_{e,\widehat{r}+})$  denote the diagonal matrix of the corresponding denoised singular values. The final estimator is then given by

$$\widehat{S}_{e\mathcal{O}\mathcal{W}\mathcal{S}} := \widehat{U}_{\widehat{\varphi}_e^*} \widehat{D}_{\widehat{\varphi}_e^*} \widehat{V}_{\widehat{\varphi}_e^*}^\top, \quad (15)$$

which incorporates both denoised singular values and singular vectors, yielding a more accurate approximation of the original clean matrix  $S$ .

### 1.3.1 Outlines

The structure of the paper is as follows. Section 2 reviews the relevant background of  $\mathcal{O}\mathcal{S}$  and  $\mathcal{W}\mathcal{S}$  necessary for subsequent developments. Section 3 introduces the theoretical results of the first-order perturbation of singular vectors and the variance of the eGHWT coefficients  $\langle \widehat{S}_{\widehat{\varphi}_e}, \Phi_{(\mathbf{p}, \mathbf{q})} \rangle$  for any basis function  $\Phi_{(\mathbf{p}, \mathbf{q})}$  with the noise model (3). Section 4 introduces our proposed algorithm,  $e\mathcal{O}\mathcal{W}\mathcal{S}$ , and its theoretical guarantees. Section 5 conducts a series of numerical evaluations of  $e\mathcal{O}\mathcal{W}\mathcal{S}$ , including comparisons with existing algorithms using simulated and real databases. The introduction of the Questionnaire algorithm and eGHWT, as well as additional numerical simulations, technical details, and proofs of theorems, can be found in the Appendix.

## 2 Preliminaries

### 2.1 Required Assumptions

**Definition 2.1.** Define the empirical spectral distribution of an  $n \times n$  symmetric matrix  $H$  as

$$\pi_H := \frac{1}{n} \sum_{i=1}^n \delta_{\ell_i}, \quad (16)$$

where  $\ell_1 \geq \ell_2 \geq \dots \geq \ell_n$  are the eigenvalues of  $H$  and  $\delta$  is the Dirac delta measure.

**Definition 2.2 (Integral transforms).** Denote the probability measures for the eigenvalues of  $ZZ^\top$  and  $Z^\top Z$  as  $\mu_{1c}$  and  $\mu_{2c}$ , respectively, when  $n \rightarrow \infty$ , with the corresponding continuous density functions  $\rho_{1c}$  and  $\rho_{2c}$ . Moreover, denote  $\lambda_+$  as the right edge of  $\rho_{1c}$  and  $\rho_{2c}$ . Denote the  $D$ -transform as

$$\mathcal{T}(x) := x m_{1c}(x) m_{2c}(x). \quad (17)$$

where  $m_{1c}$  and  $m_{2c}$  are the Stiltjes transform

$$m_{1c}(x) = \int_0^{\lambda+} \frac{\rho_{1c}(t)}{t-x} dt \quad \text{and} \quad m_{2c}(x) = \int_0^{\lambda+} \frac{\rho_{2c}(t)}{t-x} dt. \quad (18)$$

**Definition 2.3 (Stochastic domination).** Let  $\xi = (\xi^{(n)}(u) : n \in \mathbb{N}, u \in U^{(n)})$  and  $\zeta = (\zeta^{(n)}(u) : n \in \mathbb{N}, u \in U^{(n)})$  be two families of nonnegative random variables, where  $U^{(n)}$  is a possibly  $n$ -dependent parameter set. We say  $\xi$  is stochastically dominated by  $\zeta$ , uniformly in  $u$ , if for any fixed (small)  $\epsilon > 0$  and (large)  $D > 0$ ,  $\sup_{u \in U^{(n)}} \mathbb{P}[\xi^{(n)}(u) > n^\epsilon \zeta^{(n)}(u)] \leq n^{-D}$  for large enough  $n \geq n_0(\epsilon, D)$ , and we shall use the notation  $\xi \prec \zeta$  or  $\xi = O_{\prec}(\zeta)$ . Throughout this paper, stochastic domination will always be uniform in all parameters that are not explicitly fixed, such as matrix indices, and  $z$  that takes values in some compact set. Note that  $n_0(\epsilon, D)$  may depend on quantities that are explicitly constant, such as  $\tau$  in Assumption 2.5. Moreover, we say that an event  $\Xi$  holds with high probability if for any constant  $D > 0$ ,  $\mathbb{P}(\Xi) \geq 1 - n^{-D}$ , when  $n$  is sufficiently large.

**Definition 2.4 (Tree structure and Mixed Hölder condition).** Let  $X$  and  $Y$  denote the column and row spaces of a matrix  $S$ , respectively. Both  $X$  and  $Y$  are equipped with partition trees and are denoted by  $T_X$  and  $T_Y$ . If  $I_{x,x'}$  denotes the smallest folder in  $T_X$  containing both  $x$  and  $x'$ , then the tree distance  $d_X(x, x')$  is defined as:

$$d_X(x, x') = \begin{cases} |I_{x,x'}|, & \text{if } x \neq x' \\ 0, & \text{if } x = x' \end{cases} \quad (19)$$

Given any  $\alpha > 0$ , we say that  $S$  has a mixed Hölder( $\alpha$ ) norm  $L = L(S, \alpha)$  if the maximum of the following terms:

$$\sup_{x \neq x', y \neq y'} \frac{S(x, y) - S(x, y') - S(x', y) + S(x', y')}{d_X(x, x')^\alpha d_Y(y, y')^\alpha}, \quad (20)$$

is bounded by  $L$ . We refer to the quantity in (20) as the  $MH(L, \alpha)$  condition of  $S$ .

**Assumption 2.5.** Fix a small constant  $0 < \tau < 1$ . We need the following assumptions for the model (1):

- (i) (Assumption on  $X$ ). Suppose the entries of  $X$  are i.i.d. Gaussian random variables with mean zero and variance  $1/n$ .



(ii) (Assumptions on  $p/n$ ). Define  $\beta_n = p/n$ . Assume  $p = p(n)$  such that

$$\tau < \beta_n < \tau^{-1}. \quad (21)$$

(iii) (Assumption on  $\mathcal{A}$  and  $\mathcal{B}$ ). Assume  $\mathcal{A}$  and  $\mathcal{B}$  are deterministic symmetric matrices with eigendecompositions

$$\mathcal{A} = Q^a \Sigma^a (Q^a)^\top, \quad \mathcal{B} = Q^b \Sigma^b (Q^b)^\top \quad (22)$$

, where  $\Sigma^a = \text{diag}(\sigma_1^a, \dots, \sigma_p^a)$ , and  $\Sigma^b = \text{diag}(\sigma_1^b, \dots, \sigma_n^b)$ . Without loss of generality, we let  $\sigma_1^a \geq \sigma_2^a \geq \dots \geq \sigma_p^a$ ,  $\sigma_1^b \geq \sigma_2^b \geq \dots \geq \sigma_n^b$ ,  $Q^a \in O(p)$ , and  $Q^b \in O(n)$ . Let  $(M_{1c}(z), M_{2c}(z)) \in \mathbb{C}^+ \times \mathbb{C}^+$  as the unique solution to the following system of self-consistent equations

$$M_{1c}(z) = \beta_n \int \frac{x}{-z[1 + xM_{2c}(z)]} \pi_{\mathcal{A}}(dx), \quad M_{2c}(z) = \int \frac{x}{-z[1 + xM_{1c}(z)]} \pi_{\mathcal{B}}(dx). \quad (23)$$

We assume that for all sufficiently large  $n$ ,

$$1 + M_{1c}(\lambda_+) \sigma_1^b \geq \tau \quad \text{and} \quad 1 + M_{2c}(\lambda_+) \sigma_1^a \geq \tau \quad (24)$$

and

$$\sigma_1^a \vee \sigma_1^b \leq \tau^{-1} \quad \text{and} \quad \pi_{\mathcal{A}}([0, \tau]) \vee \pi_{\mathcal{B}}([0, \tau]) \leq 1 - \tau. \quad (25)$$

(iv) (Assumption on the signal strength). We assume

$$d_1 > d_2 > \dots > d_r > 0 \quad (26)$$

for some  $r > 1$ ,  $d_1 < \tau^{-1}$ , and the spectral gap  $\min_{i,j} |d_i - d_j| > \tau$ . Denote a fixed value  $\gamma > 0$  as

$$\gamma := 1/\sqrt{\mathcal{T}(\lambda_+)}. \quad (27)$$

We allow the singular values  $d_k$  to depend on  $n$  under the condition that there exists an integer  $1 < r^+ \leq r$ , called the effective rank of  $\tilde{S}$ , such that

$$d_k - \gamma > n^{\varepsilon-1/3} \quad \text{if and only if} \quad 1 \leq k \leq r^+, \quad (28)$$

for some  $\varepsilon > 1/6$ .

- (v) (*Assumption on the distribution of singular vectors*). Let  $G_{\mathbf{u}}^p \in \mathbb{R}^{p \times p}$  and  $G_{\mathbf{v}}^n \in \mathbb{R}^{n \times n}$  be two independent matrices with i.i.d entries distributed according to a fixed probability measure  $\nu$  on  $\mathbb{R}$  with mean zero and variance one, and satisfy the log-Sobolev inequality. For  $i = 1, \dots, p$  and  $j = 1, \dots, n$ , we assume that the left and right singular vectors,  $\mathbf{u}_i \in \mathbb{R}^p$  and  $\mathbf{v}_j \in \mathbb{R}^n$ , are the  $i$ -th column and the  $j$ -th columns obtained from the Gram-Schmidt (or QR factorization) of  $G_{\mathbf{u}}^p$  and  $G_{\mathbf{v}}^n$  respectively.
- (vi) (*Tree structure and Mixed Hölder condition on  $S$* ). Denote its row and column spaces by  $X = \{x_1, \dots, x_p\}$  and  $Y = \{y_1, \dots, y_n\}$ , where  $x_i \in \mathbb{R}^n$  is the  $i$ -th row of  $S$  and  $y_j \in \mathbb{R}^p$  is the  $j$ -th column of  $S$ .  $X$  and  $Y$  are equipped with normalized counting measure, such that the measure for any single point  $x \in X$  is  $p^{-1}$  and the measure of any single point  $y \in Y$  is  $n^{-1}$ . We assume that after the random generation of singular values and singular vectors described in (iv) and (v), the sets  $X$  and  $Y$  exhibit intrinsic hierarchical structures that can be represented by underlying trees  $T_X$  and  $T_Y$ , respectively, such that  $S$  has a mixed Hölder( $\alpha$ ) norm  $L = L(S, \alpha)$  for an  $\alpha > 0$  with respect to the equipped trees  $T_X$  and  $T_Y$  and tree distances defined in (19).
- (vii) (*Balanced partition tree*) Given a folder  $I$  in a tree, the smallest folder containing but not equal to  $I$  is called its "parent". If  $I'$  is the parent of  $I$ , we also say that  $I$  is a "child" of  $I'$ . We assume that the both partition trees  $\mathcal{T}_X$  and  $\mathcal{T}_Y$  from (vi) are balanced, meaning there are constants  $B_L$  and  $B_U$  such that:

$$0 < B_L \leq \frac{|\text{child}|}{|\text{parent}|} \leq B_U < 1. \quad (29)$$

*Remark 2.6.* Assumptions (i)–(v) follow the setup in [44] for deriving the theoretical guarantees of eOptShrink. For Assumption (i), [44] adopts a weaker condition requiring only that the entries of  $X$  have finite fourth moments. In this work, we assume that the entries of  $X$  are i.i.d. Gaussian to simplify the theoretical discussion. This assumption eliminates moment-dependent terms in (iv) of Assumption 2.5 and in the subsequently introduced Theorem 2.11 for the convergence guarantee of eOptShrink. Nevertheless, in our numerical experiments, we demonstrate that the proposed approach remains valid even when  $X$  is non-Gaussian, provided it satisfies weaker-moment conditions. Moreover, compared to the original setup in [44], Assumption (iv) is simplified to ensure the spectral gap  $\min_{i,j} |d_i - d_j| > \tau$  and Assumption (v)

is simplified to ensure that the sets  $\{\mathbf{u}_i\}$  and  $\{\mathbf{v}_i\}$  consist of orthogonal vectors. These condition facilitates variance calculation in the subsequent analysis of first-order singular vector perturbations in Theorem 3.1 3.2, and 3.3. For additional background and details of random matrix theory, we refer the reader to [11, 38, 17, 44].

Assumptions (vi) and (vii) encodes the mixed Hölder regularity condition on the matrix  $S$  and the quipped trees  $\mathcal{T}_X$  and  $\mathcal{T}_Y$  have balanced folders, which forms the basis for the theoretical guarantees of  $\mathcal{WS}$  established in [2].

## 2.2 Results of Optimal Shrinkage of Singular Values

Recall the definition of asymptotic loss and optimal shrinker provided in [26, Definitions 1 and 2] .

**Definition 2.7 (Asymptotic loss).** Let  $\mathcal{L} := \{L_{p,n} | p, n \in \mathbb{N}\}$  be a family of loss functions, where each  $L_{p,n} : M_{p \times n} \times M_{p \times n} \rightarrow [0, \infty)$  is a loss function obeying that  $\hat{S} \rightarrow L_{p,n}(S, \hat{S})$  is continuous and  $L_{p,n}(S, S) = 0$ . Suppose  $p = p(n)$  and  $\lim_{n \rightarrow \infty} p(n)/n \rightarrow \beta > 0$ . Let  $\varphi : [0, \infty) \rightarrow [0, \infty)$  be a nonlinear function and consider  $\hat{S}_\varphi$  to be the singular shrinkage estimate (2). When  $\lim_{n \rightarrow \infty} L_{p,n}$  exists, we define the asymptotic loss of the shrinker  $\varphi$  with respect to  $L_{p,n}$  with the signal  $\mathbf{d} = (d_1, \dots, d_r)$  as  $L_\infty(\varphi|\mathbf{d}) = \lim_{n \rightarrow \infty} L_{p,n}(S, \hat{S}_\varphi)$ , where  $S$  is defined in (1).

**Definition 2.8 (Optimal shrinker).** Let  $L_\infty$  and  $\varphi$  be as defined in Definition 2.7. If a shrinker  $\varphi^*$  has an asymptotic loss that satisfies  $L_\infty(\varphi^*|\mathbf{d}) \leq L_\infty(\varphi|\mathbf{d})$  for any other shrinker  $\varphi$ , any  $r \geq 1$ , and any  $\mathbf{d} \in \mathbb{R}^r$ , then we say that  $\varphi^*$  is uniquely asymptotically admissible (or simply “optimal”) for the loss family  $\mathcal{L}$  and that class of shrinkers.

From now on, we denote the optimal shrinker of  $\tilde{\lambda}_i$  as

$$\varphi_i^* := \varphi^*(\tilde{\lambda}_i). \quad (30)$$

**Proposition 2.9** ([26, 31]). When  $d_i \geq \alpha$ , the optimal shrinker is  $\varphi_i^* = d_i \sqrt{a_{1,i}^\infty a_{2,i}^\infty}$ ,  $\varphi_i^* = d_i \sqrt{\frac{a_{1,i}^\infty \wedge a_{2,i}^\infty}{a_{1,i}^\infty \vee a_{2,i}^\infty}}$  and  $\varphi_i^* = d_i (\sqrt{a_{1,i}^\infty a_{2,i}^\infty} - \sqrt{(1 - a_{1,i}^\infty)(1 - a_{2,i}^\infty)})$  when the Frobenius norm, operator norm, and nuclear norm are considered in the loss function, respectively. When  $d_i < \gamma$ , for any loss function, we have  $\varphi_i^* = 0$ .

Based on Proposition 2.9, in [44] we estimated  $d_i$ ,  $a_{1,i}^\infty$  and  $a_{2,i}^\infty$  using the eigenstructure of the noisy matrix  $\tilde{S}\tilde{S}^\top$ , and obtained estimated optimal

shrinkers based on theoretical results on biased singular values and vectors, including their limiting behavior and associated convergence rates. We refer the reader to check Theorems 3.2 and 3.3 of [44] for the convergence of singular values  $\tilde{\lambda}_i \rightarrow \mathcal{T}^{-1}(d_i^{-2})$  and Theorems 3.4 and 3.5 of [44] for the convergence of inner product  $a_{1,i} \rightarrow a_{1,i}^\infty$  and  $a_{2,i} \rightarrow a_{2,i}^\infty$ , which form the foundation of the following eOptShrink algorithm.

### 2.2.1 eOptShrink

Define

$$\mathbb{O}_+ := \{1, \dots, r^+\} \quad \text{and} \quad \Delta(d_i) := |d_i - T|^{1/2}. \quad (31)$$

Define an estimator of the bulk edge

$$\hat{\lambda}_+ := \tilde{\lambda}_{\lfloor n^c \rfloor + 1} + \frac{1}{2^{2/3} - 1} \left( \tilde{\lambda}_{\lfloor n^c \rfloor + 1} - \tilde{\lambda}_{2\lfloor n^c \rfloor + 1} \right). \quad (32)$$

Then we estimate  $r^+$  and set

$$\hat{r}^+ := \left| \{ \tilde{\lambda}_i | \tilde{\lambda}_i > \hat{\lambda}_+ + n^{-1/3} \} \right|. \quad (33)$$

The following theorems from [44] guarantee the performance of  $\hat{r}^+$ .

**Theorem 2.10** (Theorem 4.2 [44]). *Suppose (i)-(v) of Assumption 2.5 hold true. Denote the event  $\Xi(r^+) := \{\hat{r}^+ = r^+\}$  and let  $0 < c < 1/2$ . Then  $\Xi(r^+)$  is an event with high probability.*

Denote

$$\hat{\lambda}_j := \tilde{\lambda}_{\lfloor n^c \rfloor + \hat{r}^+ + 1} + \frac{1 - \left( \frac{j - \hat{r}^+ - 1}{\lfloor n^c \rfloor} \right)^{2/3}}{2^{2/3} - 1} \left( \tilde{\lambda}_{\lfloor n^c \rfloor + \hat{r}^+ + 1} - \tilde{\lambda}_{2\lfloor n^c \rfloor + \hat{r}^+ + 1} \right), \quad (34)$$

The estimated CDF of  $\pi_{ZZ^\top}$  in [44] is

$$\hat{F}_e(x) := \frac{1}{p - \hat{r}^+} \left( \sum_{j=\hat{r}^++1}^{\lfloor n^c \rfloor + \hat{r}^+} \mathbb{1}(\hat{\lambda}_j \leq x) + \sum_{j=\lfloor n^c \rfloor + \hat{r}^+ + 1}^p \mathbb{1}(\tilde{\lambda}_j \leq x) \right). \quad (35)$$

For  $1 \leq i \leq \hat{r}^+$ , denote the estimators of  $m_{1c}(\tilde{\lambda}_i)$  and  $m_{2c}(\tilde{\lambda}_i)$  as

$$\begin{aligned} \hat{m}_{e,1,i} &:= \int \frac{d\hat{F}_e(x)}{x - \tilde{\lambda}_i} = \frac{1}{p - \hat{r}^+} \left( \sum_{j=\hat{r}^++1}^{\lfloor n^c \rfloor + \hat{r}^+} \frac{1}{\hat{\lambda}_j - \tilde{\lambda}_i} + \sum_{j=\lfloor n^c \rfloor + \hat{r}^+ + 1}^p \frac{1}{\tilde{\lambda}_j - \tilde{\lambda}_i} \right), \\ \hat{m}_{e,2,i} &:= \frac{1 - \beta_n}{\tilde{\lambda}_i} + \beta_n \hat{m}_{e,1,i}. \end{aligned} \quad (36)$$

For  $1 \leq i \leq \hat{r}^+$ , the estimator of the  $D$ -transform  $\mathcal{T}(\tilde{\lambda}_i)$  is

$$\hat{\mathcal{T}}_{e,i} = \tilde{\lambda}_i \hat{m}_{e,1,i} \hat{m}_{e,2,i}, \quad (37)$$

and the estimators of  $d_i$  and inner products of the clean and noisy left singular vectors  $a_{1,i}$  and right singular vectors  $a_{2,i}$ , are given by

$$\hat{d}_{e,i} = \sqrt{\frac{1}{\hat{\mathcal{T}}_{e,i}}}, \quad \hat{a}_{e,1,i} = \frac{\hat{m}_{e,1,i}}{\hat{d}_{e,i}^2 \hat{\mathcal{T}}_{e,i}'}, \quad \text{and} \quad \hat{a}_{e,2,i} = \frac{\hat{m}_{e,2,i}}{\hat{d}_{e,i}^2 \hat{\mathcal{T}}_{e,i}'}. \quad (38)$$

As a result, we estimate the optimal shrinker  $\varphi_i^*$  in Proposition 2.9 by

$$\begin{aligned} \hat{\varphi}_{\mathbf{e},i} &= \hat{d}_{e,i} \sqrt{\hat{a}_{\mathbf{e},1,i} \hat{a}_{\mathbf{e},2,i}}, & (\text{Frobenius norm}) \\ \hat{\varphi}_{\mathbf{e},i} &= \hat{d}_{e,i} \sqrt{\frac{\hat{a}_{e,1,i} \wedge \hat{a}_{e,2,i}}{\hat{a}_{e,1,i} \vee \hat{a}_{e,2,i}}}, & (\text{Operator norm}) \\ \hat{\varphi}_{\mathbf{e},i} &= \hat{d}_{e,i} \left( \sqrt{\hat{a}_{\mathbf{e},1,i} \hat{a}_{\mathbf{e},2,i}} - \sqrt{(1 - \hat{a}_{\mathbf{e},1,i})(1 - \hat{a}_{\mathbf{e},2,i})} \right), & (\text{Nuclear norm}) \end{aligned} \quad (39)$$

for  $1 \leq i \leq \hat{r}^+$ , and  $\hat{\varphi}_{\mathbf{e},i} = 0$  otherwise. The following theorem provides the convergence guarantee:

**Theorem 2.11** (Theorem 4.4 of [44]). *Suppose (i)-(v) of Assumption hold true for some  $\varepsilon > 1/6$ , and  $c \in (0, 1/2)$ . For all three types of loss functions mentioned in Proposition 2.9, for  $1 \leq i \leq \hat{r}^+$ , conditional on  $\Xi(r^+)$ , we have  $|\varphi_i^* - \hat{\varphi}_{\mathbf{e},i}| \prec n^{-1/2}/\Delta(d_i)$ .*

### 2.3 Results of Wavelet Shrinkage

We introduce the theoretical results of wavelet shrinkage in this section. Let  $S$  be a mixed Hölder( $\alpha$ ) matrix with norm  $L$  as defined in Definition 2.4, and be contaminated by additive noise  $Z$  as in model (1). When  $\alpha$  and  $L$  are not specified, in [21, 22, 2], the *Wavelet Shrinkage* scheme is applied to construct an estimator from  $\tilde{S}$  over all  $\alpha > 0$ . Note that in [20, 21, 22, 2], the analysis assumes that the entries in the noise matrix  $Z$  are i.i.d. Gaussian with distribution  $\mathcal{N}(0, \sigma^2)$ . However, in our high-dimensional setting described in Assumption 2.5 (i), the variance of the noise is of order  $\mathcal{O}(n^{-1})$ . To adapt the wavelet shrinkage results to this regime, we restate that the relevant theorems with the noise matrix entries  $Z$  are i.i.d. Gaussian with distribution  $\mathcal{N}(0, \sigma^2/n)$ . Besides, in [20, 21, 22, 2], the theorems and performance guarantees are stated in terms of the normalized wavelet coefficients

by an additional factor of  $1/pn$  in (6). For consistency with our framework, we restate the relevant results in terms of unnormalized wavelet coefficients.

Expand  $S$  in a two-dimensional Haar series  $\Phi_{IJ}$  as defined in (8). Since the Haar transform is orthogonal, each observed Haar coefficient  $\langle \tilde{S}, \Phi_{IJ} \rangle$  is normally distributed around the true coefficient  $\langle S, \Phi_{IJ} \rangle$ , with variance  $\sigma^2/n$ . To have an WS estimator of  $\langle S, \Phi_{IJ} \rangle$  from  $\langle \tilde{S}, \Phi_{IJ} \rangle$ , Donoho and Johnstone considered the loss function

$$\frac{\mathbb{E}_\theta[(\hat{\theta} - \theta)^2]}{\delta + m_\delta^\ell(\theta)}, \quad (40)$$

where  $\hat{\theta}$  is the estimator of  $\theta$ ,  $\delta \in (0, 1)$ ,  $\ell \in (0, 2)$ , and  $m_\delta^\ell(\theta)$  is defined by

$$m_\delta^\ell(\theta) := t^\ell \min \left\{ \left( \frac{\theta}{t} \right)^2, 1 \right\}, \quad (41)$$

with  $t = \sqrt{2 \log(1/\delta)}$ . The loss function penalizes errors made at small values of  $\theta$  more than those made at large values of  $\theta$ . The wavelet shrinker defined in (9) is consistent with the structure of the loss function, as it moves  $x$  toward zero by an amount  $\min\{t, |x|\}$ , thereby applying stronger shrinkage to smaller values of  $x$ . The following corollary from [2] shows that the shrinker yields an upper-bound of the loss function:

**Corollary 2.12** (Corollary 1 [2]). *Suppose  $\tilde{\theta} \sim N(\theta, \sigma^2)$ , where  $\sigma^2$  is assumed to be known.  $\ell \in (0, 2)$ . Define the estimator of  $\theta$  to be  $\hat{\theta} = \eta_{\sigma t}(Y)$ , where  $t = \sqrt{2 \log(1/\delta)}$  and  $\delta \in (0, 1)$ . Then there is a constant  $C > 0$  such that for all  $\delta$  sufficiently small,*

$$\sup_\theta \frac{\mathbb{E}_\theta[(\hat{\theta} - \theta)^2]}{\delta + m_\delta^\ell(\theta/\sigma)} \leq C \sigma^2 \log(1/\delta)^{1-\ell/2}. \quad (42)$$

Construct the estimator of wavelet coefficient  $\langle \tilde{S}, \Phi_{IJ} \rangle$  by the shrinker  $\eta_{\frac{t\sigma}{\sqrt{n}}}$  such that

$$\hat{C}_{\Phi_{IJ}} := \eta_{\frac{t\sigma}{\sqrt{n}}}(\langle \tilde{S}, \Phi_{IJ} \rangle) \quad (43)$$

for nonconstant tensor Haar functions  $\Phi_{IJ}$ , and  $\hat{C}_1 = \langle \tilde{S}, 1 \rangle$  and construct the estimator using the shrinker as

$$\hat{S}_t(x, y) = \sum_{\Phi_{IJ}} \hat{C}_{\Phi_{IJ}} \Phi_{IJ}(x, y). \quad (44)$$

A common threshold choice is  $t = t^* = \sqrt{2 \log(pn)}$  by extreme value theory, such that for  $N$  i.i.d. sub-Gaussian random variables, the maximum of their absolute values concentrates around  $C\sqrt{\log N}$  for some constant  $C$  (e.g. Exercise 2.5.10 [47]). This threshold ensures that, with high probability, all noise-dominated coefficients are suppressed while signal-dominated components are retained. When  $c = \frac{2\alpha}{2\alpha+1}$  and  $\ell = 2(1 - c)$ , the following theorem from [2] follows directly from Corollary 2.12 and provides a theoretical guarantee for the performance of  $\hat{S}_{t^*}$ .

**Theorem 2.13.** *Suppose (vi)-(vii) of Assumption 2.5 hold,  $S \in MH(L, \alpha)$  for some  $\alpha > 0$ , and entries of  $Z$  are i.i.d. normally distributed with mean 0 and variance  $\sigma^2/n$ . With  $t^* = \sqrt{2 \log(pn)}$ , we have:*

(1) (Section 4.1 [2]. Mean squared error of  $\hat{S}_{t^*}$ .)

$$\begin{aligned} \mathbb{E}_S \left\| S - \hat{S}_{t^*} \right\|_{2,n}^2 \\ \leq C \log^{2\alpha/(2\alpha+1)}(pn) (\sigma^2 L^{1/\alpha} / (pn^2))^{2\alpha/(2\alpha+1)} \log_{B_U^{-1}}(pn^2 L / \sigma^2) (1 + o(1)), \end{aligned} \quad (45)$$

with  $C = C(B_L, B_U, \alpha)$ .

(2) (Section 4.2 [2]. Pointwise squared error of  $\hat{S}_{t^*}$ .)

For any  $(x_0, y_0) \in X \times Y$ , we have

$$\begin{aligned} \mathbb{E}(S(x_0, y_0) - \hat{S}_{t^*}(x_0, y_0))^2 \\ \leq C \log^{2\alpha/(2\alpha+1)}(pn) (\sigma^2 L^{1/\alpha} / (pn^2))^{2\alpha/(2\alpha+1)} \log_{B_U^{-1}}^2(pn^2 L / \sigma^2) (1 + o(1)), \end{aligned} \quad (46)$$

with  $C = C(B_L, B_U, \alpha)$ .

*Remark 2.14.* (a) Note that Corollary 2.12 does not depend on the way orthogonal basis  $\{\Phi_{ij}\}$  is constructed, therefore the same asymptotic result as in Theorem 2.13 holds when the Haar basis  $\Phi_{IJ}$  in (9) is replaced by the best basis  $\Phi_{(\mathbf{p}, \mathbf{q})}$  from the eGHWT. This basis captures both local and global structures in the data, leading to sparser representations with lower  $\ell_1$ -norms of the coefficients and greater energy concentration in the leading terms. In Section 5, we demonstrate through numerical experiments that the estimator achieves improved performance when using the eGHWT basis compared to the Haar basis alone. (b) Both right-hand sides of (45) and (46) converge to zero as  $n \rightarrow \infty$ . The shrinker defined in (9) does not require the parameters  $L$  or  $\alpha$ , and depends only on the noise level  $\sigma$ , making

it particularly suitable for data-driven applications where such parameters may be difficult to estimate. However, the entries of the noise matrix  $Z$  are typically not i.i.d. Gaussian, for instance, the correlated and dependent noise model in (3). In such settings, a single global parameter  $\sigma$  is insufficient to adapt to the varying noise levels across different scales in the tree structure of  $S$ . Moreover, the tree structures  $T_X$  and  $T_Y$  are often constructed directly from the raw data matrix. When the noise  $Z$  is sufficiently strong, it can distort these trees and, as a result, degrade the quality of the associated Haar-Walsh basis.

### 3 Main Results

#### 3.1 Perturbation Analysis of Singular Vectors under High-Dimensional Setup

Denote the subspace decomposition of  $S$  as

$$S = U\Sigma V^\top = U_r \Sigma_r V_r^\top + U_c \Sigma_c V_c^\top, \quad (47)$$

where  $U_r = [\mathbf{u}_1, \dots, \mathbf{u}_r]$ , associated with the  $r$  nonzero singular values, spans the column space of  $S$ , which is also called the signal subspace, and  $U_c = [\mathbf{u}_{r+1}, \dots, \mathbf{u}_p]$ , associated with zero singular values ( $\Sigma_c = 0$ ), spans the orthogonal space of  $U_r$ , which is also called the noise subspace. Similarly,  $V_r$  spans the row space of  $S$  and  $V_c$  spans the orthogonal space of  $V_r$ . The subspace decomposition of  $\tilde{S}$  is given by

$$\tilde{S} = S + Z = \tilde{U}\tilde{\Sigma}\tilde{V}^\top = \tilde{U}_r \tilde{\Sigma}_r \tilde{V}_r^\top + \tilde{U}_c \tilde{\Sigma}_c \tilde{V}_c^\top \quad (48)$$

Due to the noise perturbation  $Z$ , all the quantities in the right-hand side (RHS) of (48) differ from those in the RHS of (47). For example, we express  $\tilde{U}_r$  as  $\tilde{U}_r = [\tilde{\mathbf{u}}_1, \dots, \tilde{\mathbf{u}}_r] = A_1 U_r + \Delta U_r$ , where  $A_1 = \text{diag}(\sqrt{a_{1,1}}, \sqrt{a_{1,2}}, \dots, \sqrt{a_{1,r}})$  is the matrix of inner products of left singular vectors  $a_{1,i} = \langle \tilde{\mathbf{u}}_i, \mathbf{u}_i \rangle^2$ , and  $\Delta U_r$  denotes the perturbation of the left singular vectors that span the signal subspace. Therefore, each perturbed left singular vector can be written as  $\tilde{\mathbf{u}}_i = \sqrt{a_{1,i}} \mathbf{u}_i + \Delta \mathbf{u}_i$ , for  $i = 1, \dots, r$ , such that  $\Delta U_r = [\Delta \mathbf{u}_1, \dots, \Delta \mathbf{u}_r]$ . Similarly, we can express  $\tilde{V}_r = [\tilde{\mathbf{v}}_1, \dots, \tilde{\mathbf{v}}_r] = A_2 V_r + \Delta V_r$ , where  $A_2 = \text{diag}(\sqrt{a_{2,1}}, \dots, \sqrt{a_{2,r}})$ ,  $\Delta V_r = [\Delta \mathbf{v}_1, \dots, \Delta \mathbf{v}_r]$ , and  $\tilde{\mathbf{v}}_i = \sqrt{a_{2,i}} \mathbf{v}_i + \Delta \mathbf{v}_i$  for  $i = 1, \dots, r$ . By construction, the perturbation  $\Delta \mathbf{u}_i \perp \mathbf{u}_i$  and  $\Delta \mathbf{v}_i \perp \mathbf{v}_i$ . Under Assumption (v) in Assumption 2.5, since the singular vectors  $\mathbf{u}_i$  are mutually orthogonal, it follows that  $\Delta \mathbf{u}_i$  lies in the span of  $\{\mathbf{u}_j\}_{j \neq i}$ . Similarly,  $\Delta \mathbf{v}_i$  is a linear combination of  $\{\mathbf{v}_j\}_{j \neq i}$ . This orthogonality structure



satisfies the conditions required for the first-order perturbation analysis in Theorem 1 of [35], which we extend to accommodate our model.

**Theorem 3.1.** *Suppose (i)-(v) of Assumption 2.5 holds. A first-order approximation of the perturbation  $\Delta \mathbf{u}_i$  and  $\Delta \mathbf{v}_i$  for  $i = 1, \dots, r$  is given by*

$$\Delta \mathbf{u}_i = d_i U_r D_i U_r^\top Z \mathbf{v}_i + U_r D_i \Sigma_r V_r^\top Z^\top \mathbf{u}_i + d_i^{-1} U_c U_c^\top Z \mathbf{v}_i, \quad (49)$$

$$\Delta \mathbf{v}_i = d_i V_r D_i V_r^\top Z^\top \mathbf{u}_i + V_r D_i \Sigma_r U_r^\top Z \mathbf{v}_i + d_i^{-1} V_c V_c^\top Z^\top \mathbf{u}_i, \quad (50)$$

where  $D_i$  is a diagonal matrix of size  $r \times r$  with the  $(i, i)$ -th element being zero and  $(j, j)$ -th element being  $1/(d_i^2 - d_j^2)$ , for  $j = 1, \dots, r$ ,  $i \neq j$ .

*Proof.* Theorem 1 in [35] requires that: (1) the order of the biased singular values  $\tilde{\lambda}_i$  matches the order of  $d_i$ , which holds under our setting by Theorem 3.2 in [44]; (2) the perturbations of the singular vectors satisfy  $\Delta \mathbf{u}_i \perp \mathbf{u}_i$  and  $\Delta \mathbf{v}_i \perp \mathbf{v}_i$ , which is satisfied by construction; and (3)  $\Delta \mathbf{u}_i$  lies in the span of  $\{\mathbf{u}_j\}_{j \neq i}$  and  $\Delta \mathbf{v}_i$  lies in the span of  $\{\mathbf{v}_j\}_{j \neq i}$ , which also holds as discussed prior to the theorem.

Note that the bias formulation of the singular vectors in [35] has been adapted to our setting by incorporating additional scaling factors  $\sqrt{a_{1,i}}$  and  $\sqrt{a_{2,i}}$  in front of the clean singular vectors. The remainder of the proof proceeds identically to that of Theorem 1 in [35].  $\square$

Based on the above theorem, we decompose the perturbation  $\Delta \mathbf{u}_i$  and  $\Delta \mathbf{v}_i$  as

$$\begin{aligned} \Delta \mathbf{u}_i &= \Delta \mathbf{u}_i^r + \Delta \mathbf{u}_i^c, \\ \Delta \mathbf{v}_i &= \Delta \mathbf{v}_i^r + \Delta \mathbf{v}_i^c, \end{aligned} \quad (51)$$

where

$$\begin{aligned} \Delta \mathbf{u}_i^r &:= d_i U_r D_i U_r^\top Z \mathbf{v}_i + U_r D_i \Sigma_r V_r^\top Z^\top \mathbf{u}_i, \\ &= U_r D_i U_r^\top (Z S^\top + S Z^\top) \mathbf{u}_i \\ \Delta \mathbf{u}_i^c &:= d_i^{-1} U_c U_c^\top Z \mathbf{v}_i. \\ \Delta \mathbf{v}_i^r &:= d_i V_r D_i V_r^\top Z^\top \mathbf{u}_i + V_r D_i \Sigma_r U_r^\top Z \mathbf{v}_i, \\ &= V_r D_i V_r^\top (Z^\top S + S^\top Z) \mathbf{v}_i \\ \Delta \mathbf{v}_i^c &:= d_i^{-1} V_c V_c^\top Z^\top \mathbf{u}_i. \end{aligned} \quad (52)$$

$\Delta \mathbf{u}_i^r$  and  $\Delta \mathbf{v}_i^r$  are variation contributed from the signal subspace  $U_r$  and  $V_r$ , and  $\Delta \mathbf{u}_i^c$  and  $\Delta \mathbf{v}_i^c$  are variation contributed from the noise subspace  $U_c$  and

$V_c$ . We have the following theorem to show the statistics of the first-order perturbation of singular vectors  $\mathbf{u}_i$  and  $\mathbf{v}_i$  are dominated by the contribution from  $\Delta \mathbf{u}_i^c$  and  $\Delta \mathbf{v}_i^c$  in the high dimensional setup. The proof is provided in Appendix.

**Theorem 3.2.** *Suppose Assumption 2.5 holds. For  $i = 1, \dots, r$ ,  $1 \leq a \leq p$ , and  $1 \leq b \leq n$ , when  $n$  is sufficiently large, we have*

$$\mathbb{E}[(\Delta \mathbf{u}_i)_a^2] \simeq \mathbb{E}[(\Delta \mathbf{u}_i^c)_a^2] = O(n^{-1}), \quad \mathbb{E}[(\Delta \mathbf{v}_i)_b^2] \simeq \mathbb{E}[(\Delta \mathbf{v}_i^c)_b^2] = O(n^{-1}),$$

such that

$$\mathbb{E}[(\Delta \mathbf{u}_i)_a^2] - \mathbb{E}[(\Delta \mathbf{u}_i^c)_a^2] = O(n^{-2}), \quad \mathbb{E}[(\Delta \mathbf{v}_i)_b^2] - \mathbb{E}[(\Delta \mathbf{v}_i^c)_b^2] = O(n^{-2}).$$

Based on the above theorem, we derive the following approximation of the variance for any GHWT coefficients of  $S_{\varphi_e} := \sum_{i=1}^{r^+} \frac{d_i}{\sqrt{a_{1,i}a_{2,i}}} \tilde{\mathbf{u}}^i \tilde{\mathbf{v}}_i^T$ .

**Theorem 3.3.** *Suppose Assumption 2.5 holds true. Let  $S_{\varphi_e} = \sum_{i=1}^{r^+} \frac{d_i}{\sqrt{a_{1,i}a_{2,i}}} \tilde{\mathbf{u}}^i \tilde{\mathbf{v}}_i^T$ . Given a Haar-Walsh basis  $\Phi_{(\mathbf{p}, \mathbf{q})}(x, y) = \omega_{\mathbf{p}}(x)\omega_{\mathbf{q}}(y)$ . Denote  $S_{r^+} := \sum_{i=1}^{r^+} d_i \mathbf{u}_i \mathbf{v}_i^T$ . Let  $C_{\Phi_{(\mathbf{p}, \mathbf{q})}} = \langle S_{r^+}, \Phi_{(\mathbf{p}, \mathbf{q})} \rangle$  and  $\hat{C}_{\Phi_{(\mathbf{p}, \mathbf{q})}} = \langle S_{\varphi_e}, \Phi_{(\mathbf{p}, \mathbf{q})} \rangle$ , and denote the support of  $\mathbf{p}$  on the rows as  $\text{supp}(\mathbf{p})$  and denote the support of  $\mathbf{q}$  on the columns as  $\text{supp}(\mathbf{q})$ . Define*

$$\begin{aligned} F_{\Phi_{(\mathbf{p}, \mathbf{q})}}(r^+, S_1, S_2, S_3) := & \sum_{i=1}^{r^+} \frac{1}{a_{1,i}n^2} S_1 + \frac{1}{a_{2,i}p^2} S_2 + \left( \frac{1}{a_{1,i}pn^2} + \frac{1}{a_{2,i}p^2n} \right) S_3 \\ & + \frac{d_i^{-2}}{a_{1,i}a_{2,i}} \left( \frac{1}{n} S_1 + \frac{1}{pn} S_3 \right) \left( \frac{1}{p} S_2 + \frac{1}{pn} S_3 \right), \end{aligned} \quad (53)$$

where

$$\begin{aligned} S_1 &:= \sum_{a \in \text{supp}(\mathbf{p})} \sum_{a' \in \text{supp}(\mathbf{p})} \sum_{\ell=1}^n \mathbb{E}[Z_{a,\ell} Z_{a',\ell}] \omega_{\mathbf{p}}(a) \omega_{\mathbf{p}}(a'), \\ S_2 &:= \sum_{b \in \text{supp}(\mathbf{q})} \sum_{b' \in \text{supp}(\mathbf{q})} \sum_{k=1}^p \mathbb{E}[Z_{kb} Z_{kb'}] \omega_{\mathbf{q}}(b) \omega_{\mathbf{q}}(b'), \\ S_3 &:= \sum_{k=1}^p \sum_{\ell=1}^n \mathbb{E}[Z_{k\ell}^2]. \end{aligned}$$

Then we have

$$\sigma_{\hat{C}_{\Phi_{(\mathbf{p}, \mathbf{q})}}}^2 := \mathbb{E}[(\hat{C}_{\Phi_{(\mathbf{p}, \mathbf{q})}} - C_{\Phi_{(\mathbf{p}, \mathbf{q})}})^2] \simeq F_{\Phi_{(\mathbf{p}, \mathbf{q})}}(S_1, S_2, S_3) = O(n^{-2}),$$

such that

$$\sigma_{\hat{C}_{\Phi_{(\mathbf{p}, \mathbf{q})}}}^2 - F_{\Phi_{(\mathbf{p}, \mathbf{q})}}(S_1, S_2, S_3) = O(n^{-3}). \quad (54)$$

## 4 Final Algorithm

We first construct the estimators  $\hat{r}^+$ ,  $\hat{d}_{e,i}$ ,  $\hat{a}_{e,1,i}$ , and  $\hat{a}_{e,2,i}$  for  $i = 1, \dots, \hat{r}^+$ , based on eOptShrink as in (38). Let  $\hat{S}_{\hat{\varphi}_e} = \sum_{i=1}^{\hat{r}^+} \hat{\varphi}_{e,i} \tilde{\mathbf{u}}_i \mathbf{v}_i^T$  as an estimator of  $S_{\varphi_e}$ , where  $\hat{\varphi}_{e,i}$  is defined in (12). Define  $\hat{Z} := \hat{S} - \hat{S}_{\hat{\varphi}_e}$  as an estimator of the noise  $Z$ , the estimator of variance  $\sigma_{\Phi(\mathbf{p}, \mathbf{q})}$  then can be constructed as

$$\hat{\sigma}_{\Phi(\mathbf{p}, \mathbf{q})}^2 := F_{\Phi(\mathbf{p}, \mathbf{q})}(\hat{r}^+, \hat{S}_1, \hat{S}_2, \hat{S}_3), \quad (55)$$

where

$$\begin{aligned} \hat{S}_1 &:= \sum_{a \in \text{supp}(\mathbf{p})} \sum_{a' \in \text{supp}(\mathbf{p})} \sum_{\ell=1}^n \hat{Z}_{a,\ell} \hat{Z}_{a',\ell} \omega_{\mathbf{p}}(a) \omega_{\mathbf{p}}(a') \\ \hat{S}_2 &:= \sum_{b \in \text{supp}(\mathbf{q})} \sum_{b' \in \text{supp}(\mathbf{q})} \sum_{k=1}^p \hat{Z}_{kb} \hat{Z}_{kb'} \omega_{\mathbf{q}}(b) \omega_{\mathbf{q}}(b') \\ \hat{S}_3 &:= \sum_{k=1}^p \sum_{\ell=1}^n \hat{Z}_{k\ell}^2 \end{aligned}$$

We have the following theorem guarantee the performance of the estimated variance:

**Theorem 4.1.** *Let Assumption 2.5 hold. We have*

$$\sigma_{\Phi(\mathbf{p}, \mathbf{q})}^2 \simeq \hat{\sigma}_{\Phi(\mathbf{p}, \mathbf{q})}^2 = O(n^{-2}), \quad (56)$$

and

$$\sigma_{\Phi(\mathbf{p}, \mathbf{q})}^2 - \hat{\sigma}_{\Phi(\mathbf{p}, \mathbf{q})}^2 \prec n^{-2.5} / \min_i \Delta(d_i) \quad (57)$$

Based on the above theorems, we modify the shrinker in  $\mathcal{WS}$  from (9) to adapt to each coefficient in the eGHWT basis. Specifically, we apply the shrinkage operator as  $\eta_{t\sigma_{\Phi(\mathbf{p}, \mathbf{q})}}(\langle S_{\varphi_e}, \Phi(\mathbf{p}, \mathbf{q}) \rangle)$ , and approximate it in practice by  $\eta_{t\hat{\sigma}_{\Phi(\mathbf{p}, \mathbf{q})}}(\langle \hat{S}_{\hat{\varphi}_e}, \Phi(\mathbf{p}, \mathbf{q}) \rangle)$ . Moreover, as described in Theorem 3.2, the variation in the coefficients  $\langle \hat{S}_{\hat{\varphi}_e}, \Phi(\mathbf{p}, \mathbf{q}) \rangle$  is dominated by the perturbations  $\Delta \mathbf{u}_i^c$  and  $\Delta \mathbf{v}_i^c$ . Once the randomness in the signal generation process is fixed under Assumptions (iv) and (v) in Assumption 2.5, the entries of  $\Delta \mathbf{u}_i^c$  and  $\Delta \mathbf{v}_i^c$  become linear combinations of the entries of the noise matrix  $Z$ , as shown in (52). Therefore, by extreme value theory, the maximum expected magnitude of the perturbations satisfies

$$\max_{i=1, \dots, p} \mathbb{E}[\Delta \mathbf{u}_i^c] < C \sqrt{\log p} \quad \text{and} \quad \max_{i=1, \dots, n} \mathbb{E}[\Delta \mathbf{v}_i^c] < C \sqrt{\log n},$$

for some constant  $C > 0$ . Let  $Q_{0.99}(\widehat{Z})$  denote the 99% quantile of the entries of the matrix  $\widehat{Z}$ , defined as the value  $q$  such that  $\mathbb{P}(|\widehat{Z}_{ij}| \leq q) \geq 0.99$ . In our algorithm, we set  $\tau^* = Q_{0.99}(\widehat{Z}) / \|\widehat{Z}\|_{2,n}$  such that  $\tau^* \leq C \max(\sqrt{\log p}, \sqrt{\log n})$  with high probability. The desired wavelet shrinker is thus constructed as  $\eta_{\Phi_{(\mathbf{p}, \mathbf{q})}}^* := \eta_{\tau^* \widehat{\sigma}_{\Phi_{(\mathbf{p}, \mathbf{q})}}}$ . The final estimator  $\widehat{S}_{e\mathcal{O}\mathcal{W}\mathcal{S}}$  is then constructed as (15). The complete algorithm is introduced in Algorithm 1.

We have the following theorem to guarantee the performance of the estimator  $\widehat{S}_{e\mathcal{O}\mathcal{W}\mathcal{S}}$ :

**Theorem 4.2.** *Suppose Assumption 2.5 hold. We have:*

(1) *(Mean squared error of  $\widehat{S}_{e\mathcal{O}\mathcal{W}\mathcal{S}}$ .)*

$$\mathbb{E}_S \left\| S - \widehat{S}_{e\mathcal{O}\mathcal{W}\mathcal{S}} \right\|_{2,n}^2 \leq C \log^{2\alpha/(2\alpha+1)}(n) (L^{1/\alpha} n^{-4})^{2\alpha/(2\alpha+1)} \log_{B_U^{-1}}(n^4 L) (1+o(1)), \quad (58)$$

with  $C = C(\mathcal{A}, \mathcal{B}, B_L, B_U, \alpha)$ .

(2) *(Pointwise squared error of  $\widehat{S}_{e\mathcal{O}\mathcal{W}\mathcal{S}}$ .)*

For any  $(x_0, y_0) \in X \times Y$ , we have

$$\mathbb{E}(S(x_0, y_0) - \widehat{S}_{e\mathcal{O}\mathcal{W}\mathcal{S}}(x_0, y_0))^2 \leq C \log^{2\alpha/(2\alpha+1)}(n^2) (L^{1/\alpha} n^{-4})^{2\alpha/(2\alpha+1)} \log_{B_U^{-1}}^2(n^4 L) (1+o(1)), \quad (59)$$

with  $C = C(\mathcal{A}, \mathcal{B}, B_L, B_U, \alpha)$ .

*Remark 4.3.* Note that for optimal-shrinkage-based approaches, the loss functions defined in Definition 2.7 asymptotically converge to  $\mathcal{O}(1)$ , and the corresponding MSE scales as  $\mathcal{O}(n^{-2})$ . In contrast, the right-hand side (RHS) of (58) is significantly smaller than  $\mathcal{O}(n^{-2})$  when  $\alpha > 1/2$  and  $n$  is sufficiently large. This result guarantees that, under a mild smoothness condition, the proposed approach yields improved denoising performance compared to the eOptShrink algorithm alone. Furthermore, when  $p$  is the same order of  $n$ , the RHS of (58) and (59) are both substantially smaller than those of (45) and (46), respectively, which are derived using only the  $\mathcal{W}\mathcal{S}$  approach. These comparisons, together with the guarantees established in the above theorem, demonstrate that our proposed e $\mathcal{O}\mathcal{W}\mathcal{S}$  method significantly outperforms either eOptShrink or  $\mathcal{W}\mathcal{S}$  when used in isolation.

## 5 Numerical Experiment

We evaluated the performance of e $\mathcal{O}\mathcal{W}\mathcal{S}$  through (1) simulated kernel matrices under various noise models, and (2) the single-channel fetal ECG (fECG) extraction task using a semi-real database.

---

**Algorithm 1**  $\text{eOWS}$ 


---

**Input:**  $\tilde{S} = \sum_{i=1}^{p \wedge n} \sqrt{\tilde{\lambda}_i} \tilde{\mathbf{u}}_i \tilde{\mathbf{v}}_i^\top$ ; a constant  $c = \min\left(\frac{1}{2.01}, \frac{1}{\log(\log n)}\right)$ ; the choice of loss function (Frobenius, operator, or nuclear norm).

**Compute:**

- (i) The estimator  $\hat{r}^+$  for the effective rank by (33).
- (ii) The estimators  $\hat{d}_{e,i}$ ,  $\hat{a}_{e,1,i}$ , and  $\hat{a}_{e,2,i}$  in (38) and the shrinkers  $\hat{\varphi}_{e,i}$  in (39) for  $i = 1, \dots, \hat{r}^+$
- (iii)  $\hat{S}_{\hat{\varphi}_e} = \sum_{i=1}^{\hat{r}^+} \hat{d}_{e,i} / \sqrt{\hat{a}_{e,1,i} \hat{a}_{e,2,i}} \tilde{\mathbf{u}}_i \tilde{\mathbf{v}}_i^\top$  and  $\hat{Z} = \tilde{S} - \sum_{i=1}^{\hat{r}^+} \hat{\varphi}_{e,i} \tilde{\mathbf{u}}_i \tilde{\mathbf{v}}_i^\top$ .
- (iv) The row tree  $T_X$  and  $T_Y$  of  $\sum_{i=1}^{\hat{r}^+} \hat{\varphi}_{e,i} \tilde{\mathbf{u}}_i \tilde{\mathbf{v}}_i^\top$  by the Questionnaire approach in B.2.
- (v) The eGHWT best basis  $\{\Phi_{(\mathbf{p},\mathbf{q})}\}_{(\mathbf{p},\mathbf{q}) \in \mathcal{B}^*}$  induced by the tree structure  $\mathcal{T}_X$  and  $\mathcal{T}_Y$  on  $\hat{S}_{\hat{\varphi}_e}$  and eGHWT coefficients  $\hat{C}_{\Phi_{(\mathbf{p},\mathbf{q})}} = \langle \hat{S}_{\hat{\varphi}_e}, \Phi_{(\mathbf{p},\mathbf{q})} \rangle$ .
- (vi) The estimated variance of eGHWT coefficient  $\hat{\sigma}_{\Phi_{(\mathbf{p},\mathbf{q})}}^2$  as in (55).
- (vii)  $\tau^* = Q_{0.99}(\hat{Z}) / \|\hat{Z}\|_{2,n}$ .
- (viii)

$$\hat{S}_{\hat{\varphi}_e^*} = \sum_{\Phi_{(\mathbf{p},\mathbf{q})}} \eta_{\tau^* \hat{\sigma}_{\Phi_{(\mathbf{p},\mathbf{q})}}} (\hat{C}_{\Phi_{(\mathbf{p},\mathbf{q})}}) \Phi_{(\mathbf{p},\mathbf{q})},$$

and its first  $\hat{r}^+$  left and right singular vectors  $\hat{U}_{\hat{\varphi}_e^*}$  and  $\hat{V}_{\hat{\varphi}_e^*}$ , and let  $\hat{D}_{\hat{\varphi}_e^*} = \text{diag}(\hat{d}_{e,1}, \dots, \hat{d}_{e,\hat{r}^+})$ .

**Output:**

$$\hat{S}_{\text{eOWS}} := \hat{U}_{\hat{\varphi}_e^*} \hat{D}_{\hat{\varphi}_e^*} \hat{V}_{\hat{\varphi}_e^*}^\top$$


---

## 5.1 Recovery of Kernel

For simulated kernel matrices, we consider different types of noise. Suppose  $\mathcal{X} \in \mathbb{R}^{p \times n}$  has i.i.d. entries from a Student's t-distribution with 10 degrees of freedom. Set  $\mathcal{A} = Q_{\mathcal{A}} D_{\mathcal{A}} Q_{\mathcal{A}}^T \in \mathbb{R}^{p \times p}$ , where  $D_{\mathcal{A}} = \text{diag}\{\ell_1, \ell_2, \dots, \ell_p\}$ ,

$Q_{\mathcal{A}} \in O(p)$  is generated by the QR decomposition of a random  $p \times p$  matrix independent of  $\mathcal{X}$ . The same method is used to generate  $\mathcal{B} = Q_{\mathcal{B}} D_{\mathcal{B}} Q_{\mathcal{B}}^T \in \mathbb{R}^{n \times n}$ , which is independent of  $\mathcal{A}$  and  $\mathcal{X}$ . The noise matrix is given by  $Z = \frac{1}{L} \mathcal{A}^{1/2} \mathcal{X} \mathcal{B}^{1/2}$ , where  $L$  is a normalization factor chosen such that  $\|Z\|_{2,n} = \sqrt{p}$ . Under this normalization, the average variance of the entries of  $Z$  is  $1/n$ . We consider three types of noise constructions. The first one is the white noise (called TYPE1 below), where  $D_{\mathcal{A}} = I_p$  and  $D_{\mathcal{B}} = I_n$ . The second one has a separable covariance structure (called TYPE2 below) with a gap in the limiting distribution, where  $D_{\mathcal{A}} = \text{diag}\left\{\sqrt{1+9 \times \frac{1}{p}}, \sqrt{1+9 \times \frac{2}{p}}, \dots, \sqrt{1+9 \times \frac{p-1}{p}}, \sqrt{10}\right\}$  and  $D_{\mathcal{B}} = \text{diag}\left\{\sqrt{10+\frac{1}{n}}, \sqrt{10+\frac{2}{n}}, \dots, \sqrt{10+\frac{\lfloor n/4 \rfloor}{n}}, \sqrt{0.3}, \dots, \sqrt{0.3}, \sqrt{0.3}\right\}$ . The third one (called TYPE3 below) has a more complicated separable covariance structure with  $D_{\mathcal{A}} = \text{diag}\left\{\exp(\frac{1}{p}), \exp(\frac{2}{p}), \dots, \exp(\frac{p-1}{p}), \exp(1)\right\}$  and  $D_{\mathcal{B}} = \text{diag}\left\{1.1+\sin(4\pi(\frac{1}{n})), 1.1+\sin(4\pi(\frac{2}{n})), \dots, 1.1+\sin(4\pi(\frac{n-1}{n})), 1.1+\sin(4\pi)\right\}$ . The signal matrices  $S = \sum_{i=1}^r d_i \mathbf{u}_i \mathbf{v}_i^T$  are generated from (1) acoustic wave propagation; (2) simulated fECG. Detailed descriptions of each data model are provided in the following sections.

For each numerical simulation, we compare the performance of eOpt-Shrink,  $\mathcal{WS}$ , and e $\mathcal{OWS}$ . For  $\mathcal{WS}$ , since the noise matrix  $Z$  is normalized such that the average variance of its entries is  $1/n$ , we apply  $\mathcal{WS}$  under the assumption that the wavelet coefficients follow a Gaussian distribution  $\mathcal{N}(0, 1/n)$ , such that the shrinker is set to  $\eta_{\sqrt{2 \log(pn)/n}}$ . For eOpt-Shrink, we select the shrinker that minimizes the asymptotic Frobenius loss, thereby also minimizing the MSE. For all estimators with their SVD, e.g.,  $\hat{S} = \sum_{i=1}^{p \wedge n} \hat{d}_i \hat{\mathbf{u}}_i \hat{\mathbf{v}}_i^T$  with singular values ordered as  $\hat{d}_1 \geq \hat{d}_2 \geq \dots \geq \hat{d}_{p \wedge n}$ , we evaluate their MSE as defined in (11) with respect to the ground truth matrix  $S$ . In addition, we assess the recovery of the singular vectors corresponding to the smallest retained signal component  $\hat{d}_{\hat{r}+}$ . Specifically, we compute the projection of the estimated left singular vector  $\hat{\mathbf{u}}_{\hat{r}+}$  onto the true subspace  $U_{\hat{r}+} := [\mathbf{u}_1, \dots, \mathbf{u}_{\hat{r}+}]$ , quantified by  $\|\langle U_{\hat{r}+}, \hat{\mathbf{u}}_{\hat{r}+} \rangle\|_F$ , and similarly, the projection of the estimated right singular vector  $\hat{\mathbf{v}}_{\hat{r}+}$  onto the subspace  $V_{\hat{r}+} := [\mathbf{v}_1, \dots, \mathbf{v}_{\hat{r}+}]$ , given by  $\|\langle V_{\hat{r}+}, \hat{\mathbf{v}}_{\hat{r}+} \rangle\|_F$ . We refer to these as the “left inner product” and “right inner product,” respectively. These metrics serve as indicators of how accurately each estimator recovers the singular vectors associated with the smallest detectable signal component.

We perform simulations with increasing matrix sizes  $n = 256, 512, 1024, 2048$ , and  $4096$ , and for each  $n$ , we run 10 independent trials. To assess

comparative performance, we report the median with interquartile range error bars. Paired  $t$ -tests are conducted to evaluate statistical significance. A result is considered statistically significant if the  $p$ -value is less than 0.005.

### Experiment 1: Acoustic Waves

Consider an acoustic wave propagation scenario between two point clouds embedded in  $\mathbb{R}^3$ . The "acoustic" interaction between source  $\{x_i\}_{i=1}^p$  and target  $\{y_j\}_{j=1}^n$  is modeled by the kernel

$$S_{ij} = \frac{C \cos(2\pi\nu\|x_i - y_j\|)}{\|x_i - y_j\|}, \quad (60)$$

where  $\nu$  is the frequency parameter. This kernel corresponds to the real part of the Green's function of the three-dimensional Helmholtz equation with wavenumber  $k = 2\pi\nu$ , and  $C$  is a constant that represents the amplitude. It captures oscillatory wave behavior with spatial decay and is commonly used to model time-harmonic acoustic interactions in free space. We examine the scenario with the equispaced helical source points  $\{x_i\}_{i=1}^p$  (blue) and the non-equispaced target points  $\{y_j\}_{j=1}^n$  (red) randomly-uniformly sampled on the sheet, as illustrated in Figure 1. Since  $\{x_i\}_{i=1}^p$  and  $\{y_j\}_{j=1}^n$  are well-separated, the kernel naturally satisfies the mixed Hölder( $\alpha$ ) condition and is low-rank due to the regularity in the target and source domains. We examine  $\nu = 1$  with  $C$  selected to normalize the matrix such that  $\|S\|_F^2 = 150$  and  $p = n$ , where  $n = 256, 512, 1024, 2048$ , and 4096. The noise matrix  $Z$  of TYPE1, TYPE2, and TYPE3 are added, respectively, to the clean kernel  $S$  such that the noisy kernel is  $\tilde{S} = S + Z$ .

We apply the proposed Algorithm 1 to construct the estimator  $\hat{S}_{eOWS}$  from the noisy matrix  $\tilde{S}$ . Figure 2 shows a comparison of our estimator  $\hat{S}_{eOWS}$  with the denoised matrix  $\hat{S}_{WS}$  obtained via  $WS$ , the eOptShrink estimator  $\hat{S}_{eOptShrink}$ , the noisy observation  $\tilde{S}$ , and the ground truth matrix  $S$ , when TYPE3 noise is contaminated and  $p = n = 512$ , where rows and columns are reorganized by applying the Questionnaire algorithm (Algorithm 2) on  $\hat{S}_{eOptShrink}$ . The Questionnaire algorithm reveals the local smooth structure of each matrix. The estimator  $\hat{S}_{WS}$  tends to oversmooth certain regions due to the incorrect use of a global variance estimate under the assumption of i.i.d. Gaussian noise. In contrast, the actual noise matrix  $Z$  is correlated and dependent, satisfying a higher-moment condition. Both eOptShrink and our proposed extension, eOWS, produce more accurate denoised results, with eOWS demonstrating superior recovery by better capturing the local piecewise-smooth structure of the signal.

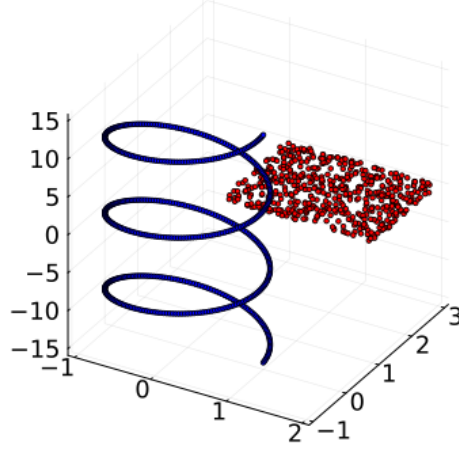


Figure 1: spatial layout of the helix (blue points  $\{x_i\}_{i=1}^p$ ) and the flat sheet (red points  $\{y_j\}_{j=1}^n$ ) for generating the kernel  $\frac{C \cos(2\pi\|x_i - y_j\|)}{\|x_i - y_j\|}$ .

Figure 3 shows the denoising performance of eOptShrink,  $\mathcal{WS}$ , and e $\mathcal{OWS}$  on the Helmholtz kernel under TYPE1, TYPE2, and TYPE3 noise. Across all values of  $n$ , e $\mathcal{OWS}$  achieves the lowest MSE and the highest left and right inner products compared to the other two approaches, with statistical significance. For all methods, the MSE decreases toward zero as  $n$  increases, with e $\mathcal{OWS}$  exhibiting a faster convergence rate. The values of the left and right inner products converge to 1 as  $n$  increases for TYPE1 and TYPE2 noise. Note that for TYPE3 noise, a drop in inner product values is observed at  $n = 2048$ . This is because, as  $n$  grows, the estimated effective rank  $\hat{r}^+$  becomes more accurate, leading to the identification of a weaker signal component from the data matrix. Nevertheless, the inner product values ultimately converge to 1 as  $n$  increases further.

## Experiment 2: Sinusoidal Waves

In this experiment, we construct the signal matrix  $S = UDV^\top \in \mathbb{R}^{n \times 2n}$ , where the entries of  $U$  are defined by sine waves:

$$U_{ij} = \sin(2\pi j x_i), \quad \text{for } i = 1, \dots, n, \quad j = 1, \dots, 10,$$



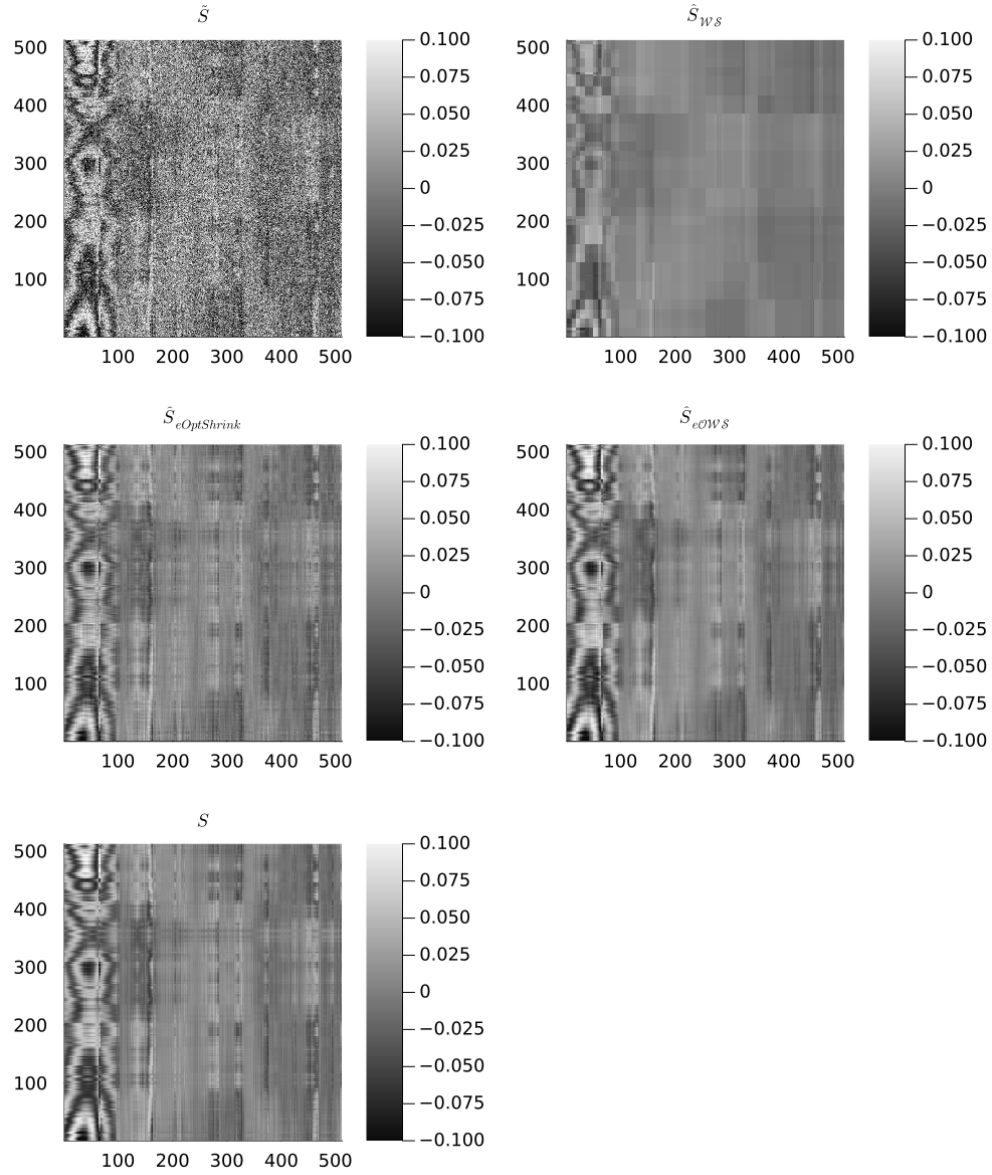


Figure 2: Comparison of denoised Helmholtz kernels. Top-left: the noisy kernel  $\tilde{S}$  contaminated with TYPE3 noise. Top-right: denoised result using  $WS$ . Middle-left: denoised result using  $eOptShrink$ . Middle-right: denoised result using  $eOWS$ . Bottom-left: the clean ground-truth kernel  $S$ .

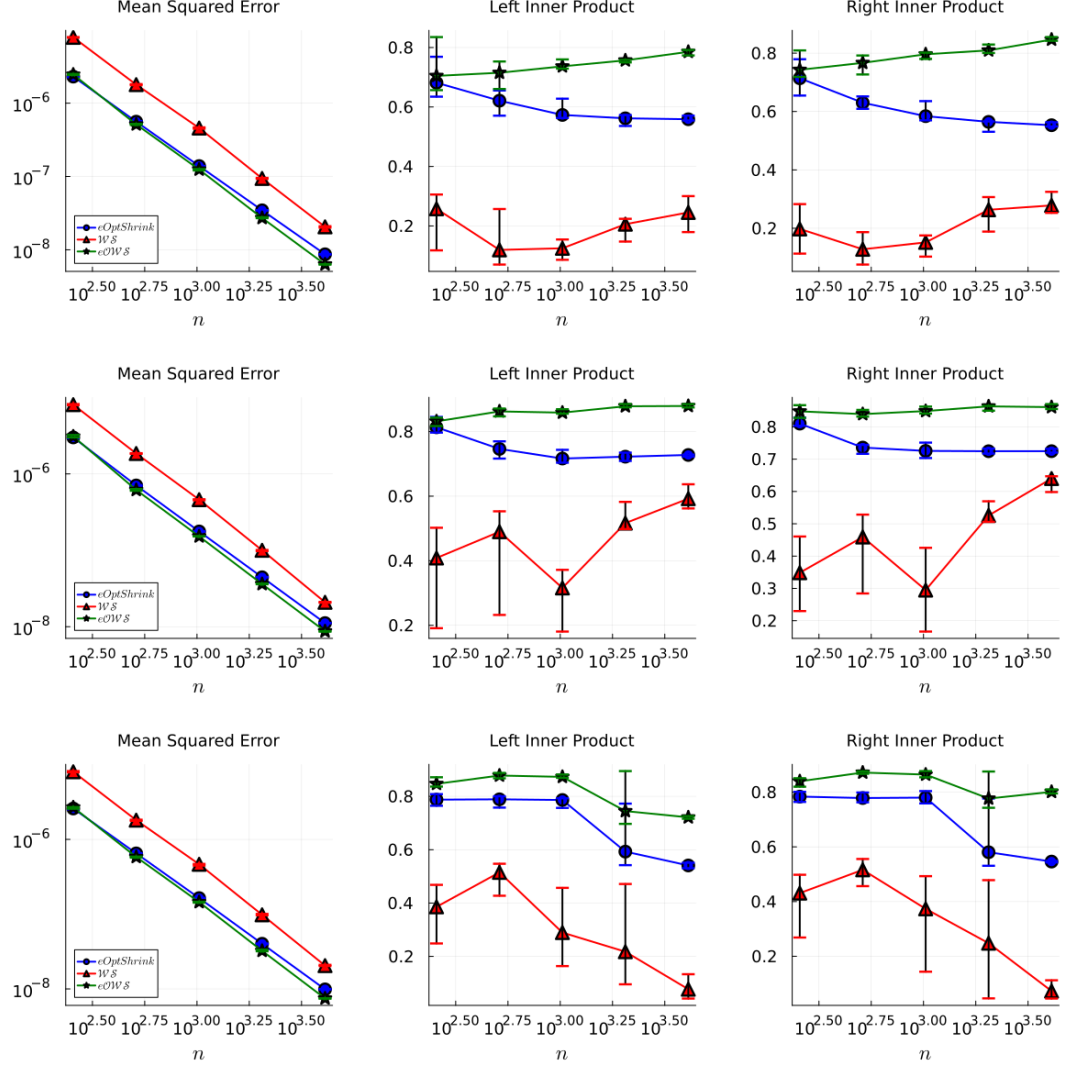


Figure 3: Comparison of the denoising performance of eOptShrink,  $\mathcal{WS}$ , and eOWS on the Helmholtz kernel. The top, middle, and bottom rows correspond to the contamination with TYPE1, TYPE2, and TYPE3 noise, respectively. The first column displays the MSE with the  $y$ -axis on a log scale, the second column shows the left inner product, and the third column presents the right inner product. The  $x$ -axis in all plots represents the value of  $n$  on a log scale. The blue circles mark the results of eOptShrink, the red triangles represent  $\mathcal{WS}$ , and the green stars denote eOWS.

with  $x_i \sim \mathcal{U}[0, 1]$  sampled independently. This gives  $U \in \mathbb{R}^{n \times 10}$ . The entries of  $V \in \mathbb{R}^{2n \times 10}$  are defined by cosine waves:

$$V_{k\ell} = \cos(2\pi\ell y_k), \quad \text{for } k = 1, \dots, 2n, \ell = 1, \dots, 10,$$

where  $y_k \sim \mathcal{U}[0, 1]$  are also sampled independently. The diagonal matrix  $D = \text{diag}(1, 2, \dots, 10)$  contains the singular values. Therefore, the signal matrix  $S$  has approximate rank 10 and exhibits an underlying smooth structure, provided that  $\{x_i\}_{i=1}^n$  and  $\{y_k\}_{k=1}^{2n}$  are well organized.

Similar to the previous experiment, we apply the proposed Algorithm 1 to construct the estimator  $\hat{S}_{eOWS}$  from the noisy matrix  $\tilde{S}$ . Figure 2 presents a comparison between our estimator  $\hat{S}_{eOWS}$ , the denoised matrix  $\hat{S}_{WS}$  obtained via  $WS$ , the eOptShrink estimator  $\hat{S}_{eOptShrink}$ , the noisy observation  $\tilde{S}$ , and the ground truth matrix  $S$ , under TYPE2 noise with  $n = 512$ . The rows and columns in all matrices are reorganized using Algorithm 2 applied to  $\hat{S}_{eOptShrink}$ . As shown, eOWS demonstrates superior recovery performance by more effectively capturing the local piecewise-smooth structure of the signal. Figure 5 shows the denoising performance of eOptShrink,  $WS$ , and eOWS on the sinusoidal waves under TYPE1, TYPE2, and TYPE3 noise. As  $n$  grows, eOWS achieves the lowest MSE and the highest left and right inner products compared to the other two approaches, with statistical significance.

## 5.2 Fetal ECG extraction problem

In our previous work [42],  $OS$  was identified as a critical step in recovering the maternal and fetal ECG (mECG and fECG) when only one or two ta-mECG channels are available. Later, in [44], we demonstrated that eOptShrink outperforms  $OS$  in morphology recovery by accounting for a more general separable covariance structure in the noise matrix.

The algorithm consists of two main steps. The first step is primarily designed for two-channel recordings and is omitted when only a single channel is available. The second step comprises two substeps: Step 2-1 detects maternal R peaks from the single-channel ta-mECG and is independent of  $OS$ ; in Step 2-2, the fECG is treated as noise and the mECG as the target signal.  $OS$  or eOptShrink is then applied to recover the mECG from the ta-mECG. After subtracting the estimated mECG from the ta-mECG, Steps 2-1 and 2-2 are repeated on the residual signal to detect fetal R-peak locations and recover the fECG. Since both the fECG (when treated as noise) and the background noise are not white and may exhibit dependencies across segments, eOptShrink demonstrates superior performance compared to  $OS$ .

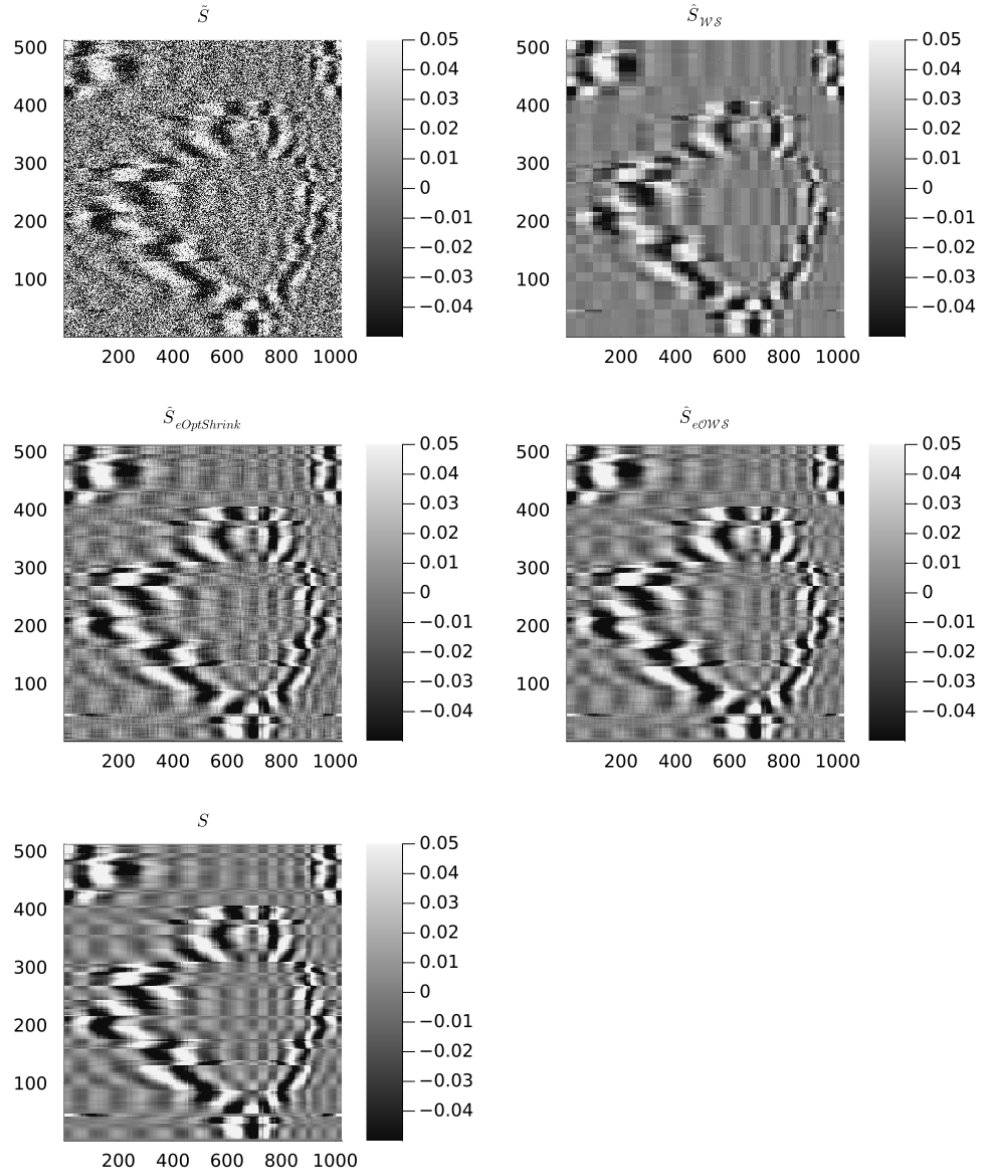


Figure 4: Comparison of denoised Sinusoidal waves. Top-left: the noisy kernel  $\tilde{S}$  contaminated with TYPE2 noise. Top-right: denoised result using  $WS$ . Middle-left: denoised result using  $eOptShrink$ . Middle-right: denoised result using  $eOWS$ . Bottom-left: the clean ground-truth kernel  $S$ .

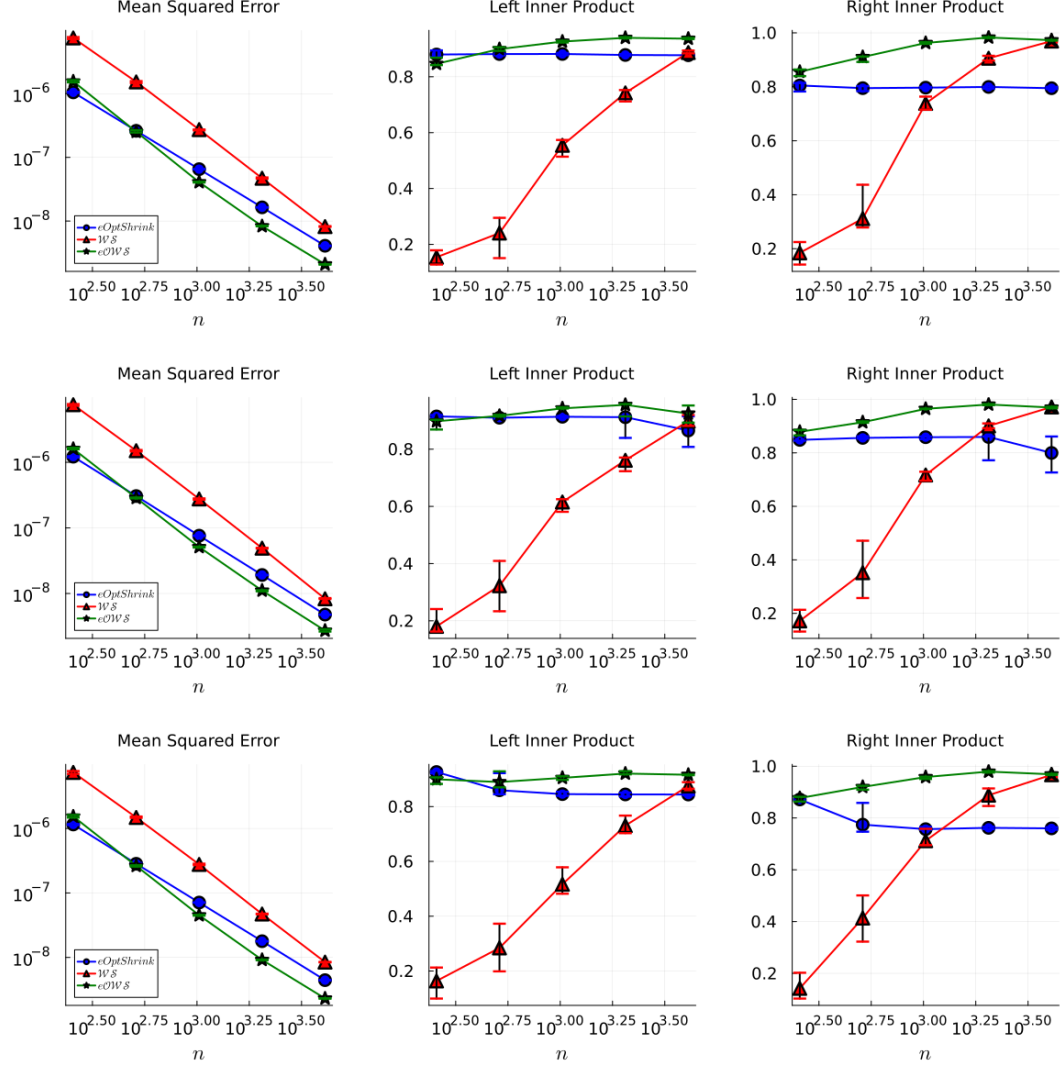


Figure 5: Comparison of the denoising performance of  $eOptShrink$ ,  $WS$ , and  $eOWS$  on the matrix of sinusoidal waves. The top, middle, and bottom rows correspond to the contamination with TYPE1, TYPE2, and TYPE3 noise, respectively. The first column displays the MSE with the  $y$ -axis on a log scale, the second column shows the left inner product, and the third column presents the right inner product. The  $x$ -axis in all plots represents the value of  $n$  on a log scale. The blue circles mark the results of  $eOptShrink$ , the red triangles represent  $WS$ , and the green stars denote  $eOWS$ .

[44]. We refer the reader to [42, 43, 44] for additional details on the ECG recovery framework.

### Semi-Real Simulated Database

To demonstrate that *eOWS* provides a further improvement in morphology recovery performance, we consider a semi-real simulated database following the same way detailed in [42]. The data is constructed from the Physikalisch-Technische Bundesanstalt (PTB) Database [12] (<https://physionet.org/physiobank/database/ptbdb/>), abbreviated as PTBDB. The database contains 549 recordings from 290 subjects (one to five recordings for one subject) aged 17 to 87 with the mean age 57.2. 52 out of 290 subjects are healthy. Each recording includes simultaneously recorded conventional 12 lead and the Frank lead ECGs. Each signal is digitalized with the sampling rate 1000 Hz. More technical details can be found online. Take 57-second Frank lead ECGs from a healthy recording, denoted as  $V_x(t)$ ,  $V_y(t)$  and  $V_z(t)$  at time  $t \in \mathbb{R}$ , as the maternal vectocardiogram (VCG). Take  $(\theta_{xy}, \theta_z) = (\frac{\pi}{4}, \frac{\pi}{4})$ , and the simulated mECG is created by  $\text{mECG}(t) = (V_x(t) \cos \theta_{xy} + V_y(t) \sin \theta_{xy}) \cos \theta_z + V_z(t) \sin \theta_z$ . We create 40 mECGs. The *simulated fECG* of healthy fetus are created from another 40 recordings from healthy subjects, where 114-second V2 and V4 recordings are taken. The simulated and simulated fECG come from different subjects. The simulated fECG then are resampled at 500 Hz. As a result, the simulated fECG has about double the heart rate compared with the simulated mECG if we consider both signals sampled at 1000 Hz. The amplitude of the simulated fECG is normalized to the same level of simulated mECG and then multiplied by  $0 < R < 1$  shown in the second column of Table 1 to make the amplitude relationship consistent with the usual situation of real ta-mECG signals. We generate 40 simulated healthy fECGs. The clean simulated ta-mECG is generated by directly summing simulated mECG and fECG. We then create a simulated noise starting with a random vector  $\mathbf{x} = (x_1, x_2, x_3, \dots)$  with i.i.d entries with student t-10 distribution. The noise is then created and denotes as  $\mathbf{z}$  with the entries  $z_i = (1 + 0.5 \sin((i \bmod 500)/500))(x_i + x_{i+1} + x_{i+2})$ . The final simulated ta-mECG is generated by adding the created noise to the clean simulated ta-mECG according to the desired SNR ratio shown in the first column of Table 1. As a result, for each combination of the fECG amplitude  $R$  and SNR, we acquire 40 recordings of 57 seconds simulated ta-mECG signals with the sampling rate 1000 Hz, and each recording has  $5.7 \times 10^4$  data points.

We apply *WS*, *eOptShrink*, and *eOWS* to each recording in the sim-

ulated database in Step 2-2 and compare its performance with  $\mathcal{WS}$  and eOptShrink. We apply  $\mathcal{WS}$  under the assumption that the wavelet coefficients follow a Gaussian distribution  $\mathcal{N}(0, 1/n)$ , such that the shrinker is set to  $\eta\sqrt{2\log(pn)/n}$ . eOptShrink is applied using the shrinker with respect to the Frobenius norm loss. For each recording, the root mean squared error (RMSE) between the reconstructed fECG cycle and the corresponding ground truth cycle is computed when the detected fetal R-peak falls within a 50ms matching window of the true R-peak location. These RMSEs are then aggregated across 40 recordings.

We report the mean  $\pm$  standard deviation, as presented in Table 1, and perform paired  $t$ -tests to assess the statistical significance of performance differences between methods, considering  $p < 0.005$  as significant. Across varying overall SNR levels and fECG amplitudes, e $\mathcal{OWS}$  consistently achieves lower RMSEs with statistical significance.

Figure 6 shows a segment of raw fECG (obtained by subtracting the reconstructed maternal ECG from the original noisy ta-mECG), the reconstructed fECG from this segment, as well as the ground truth ECG, from one subject in the simulated database. In the raw fECG, the segment from 38s to 39.5s exhibits higher noise variation, while the segment from 39.5s to 40.5s is less noisy and clearly displays a fetal ECG cycle. All three methods,  $\mathcal{WS}$ , eOptShrink, and e $\mathcal{OWS}$ , are applied to denoise this segment. Due to its inaccurate estimation of the noise level,  $\mathcal{WS}$  oversmooths the entire segment, resulting in no discernible fECG morphology. eOptShrink provides a more accurate reconstruction of the fECG morphology; however, in the 38s to 39.5s portion, the recovered signal contains stronger residual noise compared to the 39.5s to 40.5s portion, due to increased noise in the associated singular vectors. In contrast, e $\mathcal{OWS}$  achieves further denoising and yields a clearer morphological structure across both the noisy and cleaner segments.

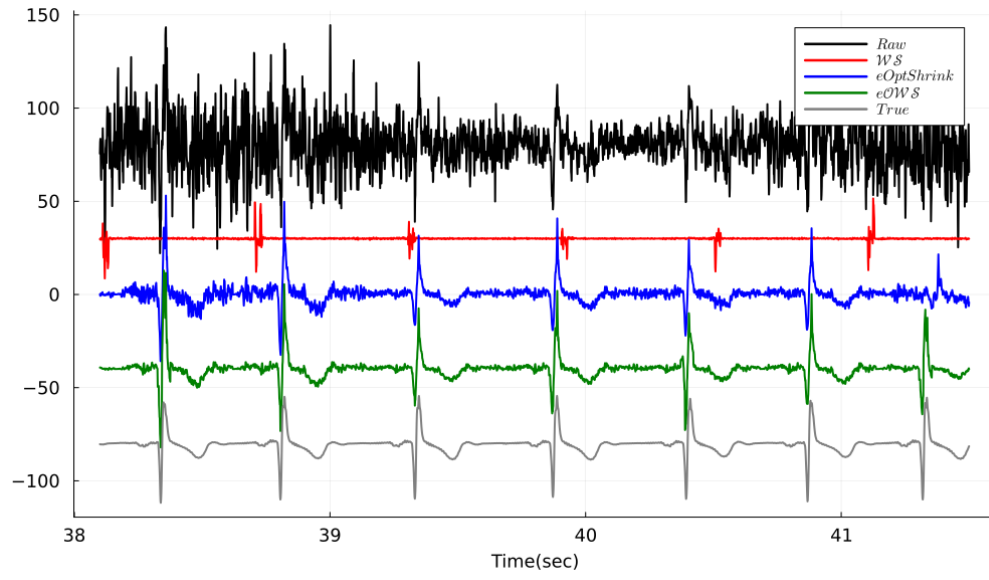


Figure 6: fECG reconstruction from a segment of the semi-real database. The black line represents the raw fECG. The red, blue, and green lines correspond to the reconstructed fECG obtained using  $\mathcal{WS}$ ,  $\text{eOptShrink}$ , and  $\text{eOWS}$ , respectively. The gray line indicates the ground truth fECG.



SNR	$R$	$\mathcal{WS}$	eOptShrink[44]	e $\mathcal{OWS}$
1 dB	1/4	108.83 $\pm$ 21.63	44.30 $\pm$ 16.99	43.31* $\pm$ 18.93
	1/6	72.84 $\pm$ 15.72	30.74 $\pm$ 12.68	29.83* $\pm$ 14.10
	1/8	54.44 $\pm$ 11.07	23.79 $\pm$ 10.03	23.13* $\pm$ 10.26
0 dB	1/4	109.44 $\pm$ 23.34	45.81 $\pm$ 17.03	43.27* $\pm$ 18.54
	1/6	73.17 $\pm$ 14.64	31.87 $\pm$ 12.11	30.40* $\pm$ 12.33
	1/8	54.66 $\pm$ 11.15	24.65 $\pm$ 9.57	23.37* $\pm$ 10.16
-1 dB	1/4	110.79 $\pm$ 23.3	49.50 $\pm$ 18.51	46.50* $\pm$ 19.02
	1/6	73.91 $\pm$ 16.50	34.35 $\pm$ 13.50	32.53* $\pm$ 13.79
	1/8	55.32 $\pm$ 13.08	26.62 $\pm$ 10.93	25.55* $\pm$ 11.88

Table 1: The comparison of RMSE for the fECG morphology of different algorithms applied to the simulated ta-mECG database.  $R$  is the simulated fECG amplitude. All results are presented as mean  $\pm$  standard deviation. The star next to the mean stands for the smaller RMSE with statistical significance when comparing with  $\mathcal{WS}$  and eOptShrink by the paired t-test with  $p < 0.005$ .

## A Proofs of Main Results

*Proof of Theorem 3.2.* For  $1 \leq a \leq p$  and  $1 \leq b \leq n$

$$\begin{aligned}
(\Delta \mathbf{u}_i^r)_a &= \sum_{k=1}^n \sum_{j=1}^p \sum_{f=1, \dots, r, f \neq i} \frac{d_i}{d_f^2 - d_i^2} (\mathbf{u}_f)_a (\mathbf{u}_f)_j Z_{jk}(\mathbf{v}_i)_k \\
&\quad + \sum_{k=1}^p \sum_{j=1}^n \sum_{f=1, \dots, r, f \neq i} \frac{d_f}{d_f^2 - d_i^2} (\mathbf{u}_f)_a (\mathbf{v}_f)_j Z_{kj}(\mathbf{u}_i)_k \\
(\Delta \mathbf{v}_i^r)_b &= \sum_{k=1}^p \sum_{j=1}^n \sum_{f=1, \dots, r, f \neq i} \frac{d_i}{d_f^2 - d_i^2} (\mathbf{v}_f)_b (\mathbf{v}_f)_j Z_{kj}(\mathbf{u}_i)_k \\
&\quad + \sum_{k=1}^n \sum_{j=1}^p \sum_{f=1, \dots, r, f \neq i} \frac{d_f}{d_f^2 - d_i^2} (\mathbf{v}_f)_b (\mathbf{u}_f)_j Z_{jk}(\mathbf{v}_i)_k \\
(\Delta \mathbf{u}_i^c)_a &= d_i^{-1} \sum_{\ell=1}^n \sum_{k=1}^p \sum_{g=r+1}^p (\mathbf{u}_g)_a (\mathbf{u}_g)_k Z_{k,\ell}(\mathbf{v}_i)_\ell \\
(\Delta \mathbf{v}_i^c)_b &= d_i^{-1} \sum_{\ell=1}^p \sum_{k=1}^n \sum_{g=r+1}^n (\mathbf{v}_g)_b (\mathbf{v}_g)_k Z_{\ell,k}(\mathbf{u}_i)_\ell
\end{aligned}$$

Thereore,

$$\begin{aligned}
\mathbb{E}[(\Delta \mathbf{u}_i^c)_a^2] &= \mathbb{E}[d_i^{-2} \sum_{\ell=1}^n \sum_{k=1}^p \sum_{g=r+1}^p \sum_{\ell'=1}^n \sum_{k'=1}^p \sum_{g'=r+1}^p (\mathbf{u}_g)_a (\mathbf{u}_g)_k Z_{k,\ell}(\mathbf{v}_i)_\ell (\mathbf{u}_{g'})_a (\mathbf{u}_{g'})_{k'} Z_{k',\ell'}(\mathbf{v}_i)_{\ell'}] \\
&= \mathbb{E}[d_i^{-2} \sum_{\ell=1}^n \sum_{k=1}^p \sum_{g=r+1}^p (\mathbf{u}_g)_a^2 (\mathbf{u}_g)_k^2 Z_{k,\ell}^2(\mathbf{v}_i)_\ell^2] + \mathbb{E}[d_i^{-2} \sum_{\ell=1}^n \sum_{g \neq g', g=r+1}^p \sum_{g'=r+1}^p (\mathbf{u}_g)_a^2 Z_{a,\ell}^2(\mathbf{v}_i)_\ell^2 (\mathbf{u}_{g'})_a^2] \\
&= d_i^{-2} \frac{p-r}{p^2 n} \sum_{k=1}^p \sum_{\ell=1}^n \mathbb{E}[Z_{k,\ell}^2] + d_i^{-2} \frac{(p-r)(p-r-1)}{p^2 n} \sum_{\ell=1}^n \mathbb{E}[Z_{a,\ell}^2].
\end{aligned}$$

Similarly,

$$\mathbb{E}[(\Delta \mathbf{v}_i^c)_b^2] = d_i^{-2} \frac{n-r}{pn^2} \sum_{k=1}^p \sum_{\ell=1}^n \mathbb{E}[Z_{k,\ell}^2] + d_i^{-2} \frac{(n-r)(n-r-1)}{pn^2} \sum_{k=1}^p \mathbb{E}[Z_{k,b}^2].$$

Since  $\mathbb{E}[Z_{k,\ell}^2] = O(1/n)$  and  $p = O(n)$  by Assumption 2.5, both terms above are of order  $O(1/n)$ . We can show  $\mathbb{E}[(\Delta \mathbf{u}_i^r)_a^2] = O(1/n^2)$  and  $\mathbb{E}[(\Delta \mathbf{v}_i^r)_b^2] = O(1/n^2)$  follows the same approach as above, and we omit the details here. Theorem 3.2 thus follows.  $\square$

*Proof of Theorem 3.3.* We want to compute the variance  $\mathbb{E}[(\hat{C}_{\Phi(\mathbf{p}, \mathbf{q})} - C_{\Phi(\mathbf{p}, \mathbf{q})})^2]$ .

$$\mathbb{E}[(\hat{C}_{\Phi} - C_{\Phi})^2] = \mathbb{E}\left[\left(\sum_{i=1}^{r^+} d_i \langle (\tilde{\mathbf{u}}_i \tilde{\mathbf{v}}_i^T / \sqrt{a_{1,i} a_{2,i}} - \mathbf{u}_i \mathbf{v}_i^T), \Phi \rangle\right)^2\right] \quad (\#)$$

Consider the contribution from the  $i$ -th singular vector

$$\begin{aligned}
(\tilde{\mathbf{u}}_i \tilde{\mathbf{v}}_i^T / \sqrt{a_{1,i} a_{2,i}} - \mathbf{u}_i \mathbf{v}_i^T)_{a,b} &= [(\mathbf{u}_i + \Delta \mathbf{u}_i / \sqrt{a_{1,i}})(\mathbf{v}_i + \Delta \mathbf{v}_i \sqrt{a_{2,i}})^T - \mathbf{u}_i \mathbf{v}_i^T]_{a,b} \\
&= (\Delta \mathbf{u}_i \mathbf{v}_i^T)_{a,b} / \sqrt{a_{1,i}} + (\mathbf{u}_i \Delta \mathbf{v}_i^T)_{a,b} / \sqrt{a_{2,i}} + (\Delta \mathbf{u}_i \Delta \mathbf{v}_i^T)_{a,b} / \sqrt{a_{1,i} a_{2,i}} \\
&= (\Delta \mathbf{u}_i)_a (\mathbf{v}_i)_b / \sqrt{a_{1,i}} + (\mathbf{u}_i)_a (\Delta \mathbf{v}_i)_b / \sqrt{a_{2,i}} + (\Delta \mathbf{u}_i)_a (\Delta \mathbf{v}_i)_b / \sqrt{a_{1,i} a_{2,i}} \\
&\simeq (\Delta \mathbf{u}_i)_a^c (\mathbf{v}_i)_b / \sqrt{a_{1,i}} + (\mathbf{u}_i)_a (\Delta \mathbf{v}_i)_b^c / \sqrt{a_{2,i}} + (\Delta \mathbf{u}_i)_a^c (\Delta \mathbf{v}_i)_b^c / \sqrt{a_{1,i} a_{2,i}},
\end{aligned}$$

where the last inequality is by Theorem 3.2. Then  $(\#)$  becomes

$$\begin{aligned}
&\simeq \sum_{i=1}^{r^+} d_i^2 \sum_{a \in I} \sum_{b \in J} \sum_{a' \in I} \sum_{b' \in J} \mathbb{E}[(\Delta \mathbf{u}_i)_a^c (\mathbf{v}_i)_b (\Delta \mathbf{u}_i)_{a'}^c (\mathbf{v}_i)_{b'} / a_{1,i} + (\Delta \mathbf{u}_i)_a^c (\mathbf{v}_i)_b (\mathbf{u}_i)_{a'} (\Delta \mathbf{v}_i)_{b'}^c / \sqrt{a_{1,i} a_{2,i}} \\
&\quad + (\Delta \mathbf{u}_i)_a^c (\mathbf{v}_i)_b (\Delta \mathbf{u}_i)_{a'}^c (\Delta \mathbf{v}_i)_{b'}^c / \sqrt{a_{1,i}^2 a_{2,i}} + (\mathbf{u}_i)_a (\Delta \mathbf{v}_i)_b^c (\mathbf{u}_i)_{a'} (\Delta \mathbf{v}_i)_{b'}^c / a_{2,i} \\
&\quad + (\mathbf{u}_i)_a (\Delta \mathbf{v}_i)_b^c (\Delta \mathbf{u}_i)_{a'}^c (\Delta \mathbf{v}_i)_{b'}^c / \sqrt{a_{1,i} a_{2,i}^2} + (\Delta \mathbf{u}_i)_a^c (\Delta \mathbf{v}_i)_b^c (\Delta \mathbf{u}_i)_{a'}^c (\Delta \mathbf{v}_i)_{b'}^c / (a_{1,i} a_{2,i})] \Phi(a, b) \Phi(a', b'), \\
&\hspace{15em} (61)
\end{aligned}$$

where we used  $\mathbb{E}[(\mathbf{u}_i)_k(\mathbf{u}_j)_k] = 0$  and  $\mathbb{E}[(\mathbf{v}_i)_\ell(\mathbf{v}_j)_\ell] = 0$  for  $k = 1, \dots, p$  and  $\ell = 1, \dots, n$  when  $i \neq j$  to eliminate the cross terms. Now, we prepare for every term required as follows:

**A.**  $d_i^2 \mathbb{E}[(\Delta \mathbf{u}_i)_a^c(\mathbf{v}_i)_b(\Delta \mathbf{u}_i)_{a'}^c(\mathbf{v}_i)_{b'}]$  and  $d_i^2 \mathbb{E}[(\mathbf{u}_i)_a(\Delta \mathbf{v}_i)_b^c(\mathbf{u}_i)_{a'}(\Delta \mathbf{v}_i)_{b'}^c]$ .  
When  $a = a'$

$$\begin{aligned}
& d_i^2 \mathbb{E}[(\Delta \mathbf{u}_i)_a^c(\mathbf{v}_i)_b(\Delta \mathbf{u}_i)_a^c(\mathbf{v}_i)_{b'}] \\
&= \sum_{\ell=1}^n \sum_{k=1}^p \sum_{g=r+1}^p \sum_{\ell'=1}^n \sum_{k'=1}^p \sum_{g'=r+1}^p \mathbb{E}[(\mathbf{u}_g)_a(\mathbf{u}_g)_k(\mathbf{u}_{g'})_a(\mathbf{u}_{g'})_{k'} Z_{k,\ell} Z_{k',\ell'} (\mathbf{v}_i)_\ell (\mathbf{v}_i)_{\ell'} (\mathbf{v}_i)_b (\mathbf{v}_i)_{b'}] \\
&\simeq \sum_{\ell=1}^n \sum_{k=1}^p \sum_{g=r+1}^p \sum_{k'=1}^p \sum_{g'=r+1}^p \mathbb{E}[(\mathbf{u}_g)_a(\mathbf{u}_g)_k(\mathbf{u}_{g'})_a(\mathbf{u}_{g'})_{k'} Z_{k,\ell} Z_{k',\ell}] \mathbb{E}[(\mathbf{v}_i)_\ell^2] \mathbb{E}[(\mathbf{v}_i)_{b'}^2] \mathbf{1}_{b=b'} \\
&= \sum_{\ell=1}^n \sum_{k=1}^p \sum_{g=r+1}^p \sum_{k'=1}^p \sum_{g'=r+1}^p \mathbb{E}[(\mathbf{u}_g)_a(\mathbf{u}_g)_k(\mathbf{u}_{g'})_a(\mathbf{u}_{g'})_{k'} Z_{k,\ell} Z_{k',\ell}] / n^2 \mathbf{1}_{b=b'}
\end{aligned}$$

And decompose into two situations  $g = g'$  and  $g \neq g'$ . When  $g = g'$  the RHS becomes

$$\begin{aligned}
&= \sum_{\ell=1}^n \sum_{k=1}^p \sum_{g=r+1}^p \sum_{k'=1}^p \mathbb{E}[(\mathbf{u}_g)_a^2(\mathbf{u}_g)_k(\mathbf{u}_g)_{k'} Z_{k,\ell} Z_{k',\ell}] / n^2 \mathbf{1}_{b=b'} \\
&= \sum_{\ell=1}^n \sum_{k=1}^p \sum_{g=r+1}^p \mathbb{E}[(\mathbf{u}_g)_a^2(\mathbf{u}_g)_k^2 Z_{k,\ell}^2] / n^2 \mathbf{1}_{b=b'} = \frac{p-r}{p^2 n^2} \sum_{\ell=1}^n \sum_{k=1}^p \mathbb{E}[Z_{k,\ell}^2] \mathbf{1}_{b=b'} = O(1/n^2).
\end{aligned}$$

And when  $g \neq g'$  the RHS becomes

$$= \sum_{\ell=1}^n \sum_{g \neq g', g=r+1}^p \sum_{g'=r+1}^p \mathbb{E}[(\mathbf{u}_g)_a^2(\mathbf{u}_{g'})_a^2 Z_{a,\ell}^2] / n^2 \mathbf{1}_{b=b'} = \frac{(p-r)(p-r-1)}{p^2 n^2} \sum_{\ell=1}^n \mathbb{E}[Z_{a,\ell}^2] \mathbf{1}_{b=b'} = O(1/n^2).$$

In conclusion, we have

$$d_i^2 \mathbb{E}[(\Delta \mathbf{u}_i)_a^c(\mathbf{v}_i)_b(\Delta \mathbf{u}_i)_a^c(\mathbf{v}_i)_{b'}] = \left( \frac{(p-r)(p-r-1)}{p^2 n^2} \sum_{\ell=1}^n \mathbb{E}[Z_{a,\ell}^2] + \frac{p-r}{p^2 n^2} \sum_{\ell=1}^n \sum_{k=1}^p \mathbb{E}[Z_{k,\ell}^2] \right) \mathbf{1}_{b=b'} = O(1/n^2). \quad (62)$$

Besides, when  $a \neq a'$ , we have

$$\begin{aligned}
& d_i^2 \mathbb{E}[(\Delta \mathbf{u}_i^c)_a(\mathbf{v}_i)_b(\Delta \mathbf{u}_i^c)_{a'}(\mathbf{v}_i)_{b'}] \\
&= \sum_{\ell=1}^n \sum_{k=1}^p \sum_{g=r+1}^p \sum_{\ell'=1}^n \sum_{k'=1}^p \sum_{g'=r+1}^p \mathbb{E}[(\mathbf{u}_g)_a(\mathbf{u}_g)_k(\mathbf{u}_{g'})_{a'}(\mathbf{u}_{g'})_{k'}Z_{k,\ell}Z_{k',\ell'}(\mathbf{v}_i)_\ell(\mathbf{v}_i)_{\ell'}(\mathbf{v}_i)_b(\mathbf{v}_i)_{b'}] \\
&\simeq \sum_{\ell=1}^n \sum_{k=1}^p \sum_{g=r+1}^p \sum_{k'=1}^p \sum_{g'=r+1}^p \mathbb{E}[(\mathbf{u}_g)_a(\mathbf{u}_g)_k(\mathbf{u}_{g'})_{a'}(\mathbf{u}_{g'})_{k'}Z_{k,\ell}Z_{k',\ell}]/n^2 \mathbf{1}_{b=b'} \\
&= \frac{(p-r)(p-r-1)}{p^2 n^2} \sum_{\ell=1}^n \mathbb{E}[Z_{a\ell}Z_{a'\ell}] + 2 \frac{p-r}{p^2 n^2} \sum_{\ell=1}^n (\mathbb{E}[Z_{a,\ell}Z_{a',\ell}]) \mathbf{1}_{b=b'} \\
&\simeq \frac{(p-r)(p-r-1)}{p^2 n^2} \sum_{\ell=1}^n \mathbb{E}[Z_{a\ell}Z_{a'\ell}] \mathbf{1}_{b=b'} = O(1/n^2).
\end{aligned}$$

In summary,

$$\begin{aligned}
& d_i^2 \sum_{a \in I} \sum_{b \in J} \sum_{a' \in I} \sum_{b' \in J} \mathbb{E}[(\Delta \mathbf{u}_i^c)_a(\mathbf{v}_i)_b(\Delta \mathbf{u}_i^c)_{a'}(\mathbf{v}_i)_{b'}\Phi(a,b)\Phi(a',b')] \\
&= \frac{(p-r)(p-r-1)}{p^2 n^2} \sum_{a \in I} \sum_{a' \in I} \sum_{\ell=1}^n \mathbb{E}[Z_{a\ell}Z_{a'\ell}] \omega_I(a) \omega_I(a') + \frac{p-r}{p^2 n^2} \sum_{a \in I} \sum_{b \in J} \sum_{\ell=1}^n \sum_{k=1}^p \mathbb{E}[Z_{k\ell}^2] \Phi(a,b)^2 \\
&= \frac{(p-r)(p-r-1)}{p^2 n^2} \sum_{a \in I} \sum_{a' \in I} \sum_{\ell=1}^n \mathbb{E}[Z_{a\ell}Z_{a'\ell}] \omega_I(a) \omega_I(a') + \frac{p-r}{p^2 n^2} \sum_{\ell=1}^n \sum_{k=1}^p \mathbb{E}[Z_{k\ell}^2] = O(1/n^2),
\end{aligned}$$

where the last equality comes from  $\sum_{a \in I} \sum_{b \in J} \Phi(a,b)^2 = 1$ .

Similarly, we have

$$\begin{aligned}
& d_i^2 \sum_{a \in I} \sum_{b \in J} \sum_{a' \in I} \sum_{b' \in J} \mathbb{E}[(\mathbf{u}_i)_a(\Delta \mathbf{v}_i)_b(\mathbf{u}_i)_{a'}(\Delta \mathbf{v}_i)_{b'}\Phi(a,b)\Phi(a',b')] \\
&= \frac{(n-r)(n-r-1)}{p^2 n^2} \sum_{b \in J} \sum_{b' \in J} \sum_{k=1}^p \mathbb{E}[Z_{kb}Z_{kb'}] \omega_J(b) \omega_J(b') + \frac{n-r}{p^2 n^2} \sum_{\ell=1}^n \sum_{k=1}^p \mathbb{E}[Z_{k\ell}^2] = O(1/n^2).
\end{aligned}$$

**B.**  $d_i^2 \mathbb{E}[(\Delta \mathbf{u}_i)_a^c(\mathbf{v}_i)_b(\mathbf{u}_i)_{a'}(\Delta \mathbf{v}_i)_{b'}^c]$  and  $d_i^2 \mathbb{E}[(\mathbf{u}_i)_a(\Delta \mathbf{v}_i)_b^c(\mathbf{u}_i)_{a'}(\Delta \mathbf{v}_i)_{b'}^c]$ .

When  $a = a'$

$$\begin{aligned}
& d_i^2 \mathbb{E}[(\mathbf{v}_i)_b (\Delta \mathbf{u}_i^c)_a (\Delta \mathbf{v}_i^c)_{b'} (\mathbf{u}_i)_a] \\
&= \sum_{\ell=1}^n \sum_{k=1}^p \sum_{g=r+1}^p \sum_{\ell'=1}^p \sum_{k'=1}^n \sum_{g'=r+1}^n \mathbb{E}[(\mathbf{u}_g)_a (\mathbf{u}_g)_k Z_{k,\ell}(\mathbf{v}_i)_\ell (\mathbf{v}_{g'})_{b'} (\mathbf{v}_{g'})_{k'} Z_{\ell',k'}(\mathbf{u}_i)_{\ell'} (\mathbf{u}_i)_a (\mathbf{v}_i)_b] \\
&= \sum_{\ell=1}^n \sum_{g=r+1}^p \sum_{\ell'=1}^p \sum_{g'=r+1}^n \mathbb{E}[(\mathbf{u}_g)_a^2 (\mathbf{v}_{g'})_{b'}^2 Z_{a,\ell} Z_{\ell',b'} (\mathbf{u}_i)_{\ell'} (\mathbf{u}_i)_a (\mathbf{v}_i)_\ell (\mathbf{v}_i)_b] \\
&= \sum_{g=r+1}^n \sum_{g'=r+1}^p \mathbb{E}[(\mathbf{u}_g)_a^2] \mathbb{E}[(\mathbf{v}_{g'})_{b'}^2] \mathbb{E}[Z_{a,b} Z_{ab'}] \mathbb{E}[(\mathbf{v}_i)_b^2] \mathbb{E}[(\mathbf{u}_i)_a^2] = \frac{(p-r)(n-r)}{p^2 n^2} \mathbb{E}[Z_{ab} Z_{ab'}] = O(1/n^3).
\end{aligned}$$

For  $a' \neq a$ , we have

$$\begin{aligned}
& d_i^2 \mathbb{E}[(\mathbf{v}_i)_b (\Delta \mathbf{u}_i^c)_a (\Delta \mathbf{v}_i^c)_{b'} (\mathbf{u}_i)_{a'}] \\
&= \sum_{\ell=1}^n \sum_{k=1}^p \sum_{g=r+1}^p \sum_{\ell'=1}^p \sum_{k'=1}^n \sum_{g'=r+1}^n \mathbb{E}[(\mathbf{u}_g)_a (\mathbf{u}_g)_k Z_{k,\ell}(\mathbf{v}_i)_\ell (\mathbf{v}_{g'})_{b'} (\mathbf{v}_{g'})_{k'} Z_{\ell',k'}(\mathbf{u}_i)_{\ell'} (\mathbf{u}_i)_{a'} (\mathbf{v}_i)_b] \\
&= \sum_{\ell=1}^n \sum_{\ell'=1}^p \sum_{g=r+1}^n \sum_{g'=r+1}^p \mathbb{E}[(\mathbf{u}_g)_a^2] \mathbb{E}[(\mathbf{v}_{g'})_{b'}^2] \mathbb{E}[Z_{a,\ell} Z_{\ell',b'}] \mathbb{E}[(\mathbf{v}_i)_\ell (\mathbf{v}_i)_b] \mathbb{E}[(\mathbf{u}_i)_{\ell'} (\mathbf{u}_i)_{a'}] \\
&= \frac{(p-r)(n-r)}{p^2 n^2} \mathbb{E}[Z_{ab'} Z_{a',b}] = O(1/n^3).
\end{aligned}$$

Therefore,  $d_i^2 \mathbb{E}[(\Delta \mathbf{u}_i)_a (\mathbf{v}_i)_b (\mathbf{u}_i)_{a'} (\Delta \mathbf{v}_i)_{b'}] = O(1/n^3)$ . Similarly,  $d_i^2 \mathbb{E}[(\mathbf{u}_i)_a (\Delta \mathbf{v}_i)_b (\mathbf{u}_i)_{a'} (\Delta \mathbf{v}_i)_{b'}] = O(1/n^3)$ . Both are much smaller than the term from  $\mathbf{A}$ .

$$\mathbf{C.} \ d_i^2 \mathbb{E}[(\Delta \mathbf{u}_i^c)_a (\Delta \mathbf{u}_i^c)_{a'} (\Delta \mathbf{v}_i^c)_b (\Delta \mathbf{v}_i^c)_{b'}]$$

$$\begin{aligned} & d_i^2 \mathbb{E}[(\Delta \mathbf{u}_i^c)_a (\Delta \mathbf{u}_i^c)_{a'}] \\ &= \sum_{\ell=1}^n \sum_{k=1}^p \sum_{g=r+1}^p \sum_{\ell'=1}^n \sum_{k'=1}^p \sum_{g'=r+1}^p \mathbb{E}[(\mathbf{u}_g)_a (\mathbf{u}_g)_k (\mathbf{u}_{g'})_{a'} (\mathbf{u}_{g'})_{k'} Z_{k,\ell} Z_{k',\ell'} (\mathbf{v}_i)_\ell (\mathbf{v}_i)_{\ell'}] \\ &= \sum_{\ell=1}^n \sum_{g=r+1}^p \sum_{g \neq g', g'=r+1}^p \mathbb{E}[(\mathbf{u}_g)_a^2 (\mathbf{u}_{g'})_{a'}^2 Z_{a,\ell} Z_{a',\ell} (\mathbf{v}_i)_\ell^2] + \sum_{k=1}^p \sum_{\ell=1}^n \sum_{g=r+1}^p \mathbb{E}[(\mathbf{u}_g)_a^2 (\mathbf{u}_g)_k^2 Z_{k,\ell}^2 (\mathbf{v}_i)_\ell^2] \mathbf{1}_{a=a'} \\ &+ 2 \sum_{\ell=1}^n \sum_{g=r+1}^p \mathbb{E}[(\mathbf{u}_g)_a^2 (\mathbf{u}_g)_{a'}^2 Z_{a,\ell} Z_{a',\ell} (\mathbf{v}_i)_\ell^2] \mathbf{1}_{a \neq a'} \\ &= \frac{(p-r)(p-r-1)}{p^2 n} \sum_{\ell=1}^n \mathbb{E}[Z_{a,\ell} Z_{a',\ell}] + \frac{p-r}{p^2 n} \sum_{k=1}^p \sum_{\ell=1}^n \mathbb{E}[Z_{k\ell}^2] \mathbf{1}_{a=a'} + 2 \frac{p-r}{p^2 n} \sum_{\ell=1}^n \mathbb{E}[Z_{a\ell} Z_{a',\ell}] \mathbf{1}_{a \neq a'} \\ &= \frac{(p-r)(p-r-1)}{p^2 n} \sum_{\ell=1}^n \mathbb{E}[Z_{a,\ell} Z_{a',\ell}] + \frac{p-r}{p^2 n} \sum_{k=1}^p \sum_{\ell=1}^n \mathbb{E}[Z_{k\ell}^2] \mathbf{1}_{a=a'} + O(1/n^2) \end{aligned}$$

Similarly,

$$\begin{aligned} & d_i^2 \mathbb{E}[(\Delta \mathbf{v}_i^c)_b (\Delta \mathbf{v}_i^c)_{b'}] \\ &= \frac{(n-r)(n-r-1)}{pn^2} \sum_{k=1}^p \mathbb{E}[Z_{kb} Z_{kb'}] + \frac{n-r}{pn^2} \sum_{k=1}^p \sum_{\ell=1}^n \mathbb{E}[Z_{k\ell}^2] \mathbf{1}_{b=b'} + 2 \frac{n-r}{pn^2} \sum_{k=1}^p \mathbb{E}[Z_{kb} Z_{kb'}] \mathbf{1}_{b \neq b'} \\ &= \frac{(n-r)(n-r-1)}{pn^2} \sum_{k=1}^p \mathbb{E}[Z_{kb} Z_{kb'}] + \frac{n-r}{pn^2} \sum_{k=1}^p \sum_{\ell=1}^n \mathbb{E}[Z_{k\ell}^2] \mathbf{1}_{b=b'} + O(1/n^2). \end{aligned}$$

In summary, since  $\Phi(a, b) = \omega_I(a) \omega_J(b)$ ,

$$\begin{aligned} & d_i^2 \sum_{a \in I} \sum_{b \in J} \sum_{a' \in I} \sum_{b' \in J} \mathbb{E}[(\Delta \mathbf{u}_i^c)_a (\Delta \mathbf{u}_i^c)_{a'} (\Delta \mathbf{v}_i^c)_b (\Delta \mathbf{v}_i^c)_{b'} \Phi(a, b) \Phi(a', b')] \\ & \simeq d_i^{-2} \left( \frac{(p-r)(p-r-1)}{p^2 n} \sum_{a \in I} \sum_{a' \in I} \sum_{\ell=1}^n \mathbb{E}[Z_{a,\ell} Z_{a',\ell}] \omega_I(a) \omega_I(a') + \frac{p-r}{p^2 n} \sum_{k=1}^p \sum_{\ell=1}^n \mathbb{E}[Z_{k\ell}^2] \right) \\ & \quad \times \left( \frac{(n-r)(n-r-1)}{pn^2} \sum_{b \in J} \sum_{b' \in J} \sum_{k=1}^p \mathbb{E}[Z_{kb} Z_{kb'}] \omega_J(b) \omega_J(b') + \frac{n-r}{pn^2} \sum_{k=1}^p \sum_{\ell=1}^n \mathbb{E}[Z_{k\ell}^2] \right) \\ & = O(1/n^2). \end{aligned}$$

$$\mathbf{D.} \ \mathbb{E}[(\Delta \mathbf{u}_i^c)_a (\mathbf{v}_i)_b (\Delta \mathbf{u}_i^c)_{a'} (\Delta \mathbf{v}_i^c)_{b'}].$$

$$\begin{aligned}
& \mathbb{E}[(\Delta \mathbf{u}_i^c)_a(\mathbf{v}_i)_b(\Delta \mathbf{u}_i^c)_{a'}(\Delta \mathbf{v}_i^c)_{b'}] \\
&= \mathbb{E}\left[\sum_{\ell=1}^p \sum_{k=1}^n \sum_{g=r+1}^n (\Delta \mathbf{u}_i^c)_a(\Delta \mathbf{u}_i^c)_{a'} d_i^{-1}(\mathbf{v}_g)_b(\mathbf{v}_g)_k Z_{\ell,k}(\mathbf{v}_i)_b(\mathbf{u}_i)_\ell\right] \\
&= \sum_{\ell=1}^p \sum_{k=1}^n \sum_{g=r+1}^n \mathbb{E}[(\Delta \mathbf{u}_i^c)_a(\Delta \mathbf{u}_i^c)_{a'} d_i^{-1}(\mathbf{v}_g)_b(\mathbf{v}_g)_k Z_{\ell,k}] \mathbb{E}[(\mathbf{v}_i)_b(\mathbf{u}_i)_\ell] = 0,
\end{aligned}$$

because  $\mathbb{E}[(\mathbf{v}_i)_b(\mathbf{u}_i)_\ell] = 0$ .

$$\begin{aligned}
& \simeq d_i^{-2} \left( \frac{(p-r)(p-r-1)}{p^2 n} \sum_{a \in I} \sum_{a' \in I} \sum_{\ell=1}^n \mathbb{E}[Z_{a,\ell} Z_{a',\ell}] \omega_I(a) \omega_I(a') + \frac{p-r}{p^2 n} \sum_{k=1}^p \sum_{\ell=1}^n \mathbb{E}[Z_{k\ell}^2] \right) \\
& \quad \times \left( \frac{(n-r)(n-r-1)}{pn^2} \sum_{b \in J} \sum_{b' \in J} \sum_{k=1}^p \mathbb{E}[Z_{kb} Z_{kb'}] \omega_J(b) \omega_J(b') + \frac{n-r}{pn^2} \sum_{k=1}^p \sum_{\ell=1}^n \mathbb{E}[Z_{k\ell}^2] \right) \\
& = O(1/n^2).
\end{aligned}$$

In conclusion, define

$$\begin{aligned}
S_1 &:= \sum_{a \in I} \sum_{a' \in I} \sum_{\ell=1}^n \mathbb{E}[Z_{a,\ell} Z_{a',\ell}] \omega_I(a) \omega_I(a') \\
S_2 &:= \sum_{b \in J} \sum_{b' \in J} \sum_{k=1}^p \mathbb{E}[Z_{kb} Z_{kb'}] \omega_J(b) \omega_J(b') \\
S_3 &:= \sum_{k=1}^p \sum_{\ell=1}^n \mathbb{E}[Z_{k\ell}^2]
\end{aligned}$$

Based on the results from A-D, (61), and  $r \ll p, n$ , we have

$$\begin{aligned}
\mathbb{E}[(\widehat{C}_\Phi - C_\Phi)^2] &\simeq \sum_{i=1}^r \frac{1}{a_1 n^2} S_1 + \frac{1}{a_2 p^2} S_2 + \left( \frac{1}{a_1 p n^2} + \frac{1}{a_2 p^2 n} \right) S_3 \\
&\quad + \sum_{i=1}^r \frac{d_i^{-2}}{a_1 a_2} \left( \frac{1}{n} S_1 + \frac{1}{pn} S_3 \right) \left( \frac{1}{p} S_2 + \frac{1}{pn} S_3 \right) \quad (63)
\end{aligned}$$

when  $n$  is sufficiently large.  $\square$

*Proof of Theorem 4.1.* This follows directly from Theorem 2.10 and 2.11, and equations (53), (54), and (55).  $\square$

## B Iterative Metric Construction

we now introduce geometry-learning approaches that construct hierarchical trees directly from the data matrix. In particular, we review techniques based on spectral graph theory and the Questionnaire algorithm, which aim to recover intrinsic affinities and multiscale structure.

### B.1 Spectral Graph Theory

Spectral graph theory provides a powerful framework for analyzing functions defined on graphs using the eigenstructure of matrices derived from graph connectivity. Given an undirected weighted graph  $G = (V, E)$  with  $N$  nodes, we define the *edge weight matrix* (or adjacency matrix)  $W \in \mathbb{R}^{N \times N}$  such that  $W_{ij} \geq 0$  encodes the affinity or similarity between nodes  $i$  and  $j$ , with  $W_{ij} = 0$  if there is no edge between them. The *degree matrix*  $D \in \mathbb{R}^{N \times N}$  is a diagonal matrix with entries  $D_{ii} := \sum_{j=1}^N W_{ij}$ , which represents the total connection strength of node  $i$  to all other nodes. From these matrices, one defines several forms of graph Laplacians, including the unnormalized Laplacian  $L = D - W$ , the random-walk normalized Laplacian  $L_{\text{rw}} = D^{-1}L$ , and the symmetric normalized Laplacian  $L_{\text{sym}} = D^{-1/2}LD^{-1/2} = I - D^{-1/2}WD^{-1/2}$ . These Laplacians play a central role in applications such as spectral clustering, graph signal processing, and dimensionality reduction. In particular, the random-walk Laplacian is closely related to the diffusion operator used in *diffusion maps* [15], a nonlinear dimensionality reduction technique that exploits the long-time behavior of random walks on graphs. Its eigenvectors form a data-driven coordinate system that preserves the geometry of the underlying data manifold. Of particular interest is the second eigenvector of  $L_{\text{sym}}$ , known as the *Fiedler vector*, which captures the most significant nontrivial mode of variation on the graph. This vector serves as a foundational tool in our framework, guiding the construction of adaptive multiscale representations through hierarchical graph partitioning.

### B.2 Tree Structure

The main computational tool we will use to construct a coupled metric and, later, the orthonormal bases they induce, is a partition tree. By this, we mean a sequence of increasingly refined partitions, readily described by a tree. As an affinity graph only holds “local” geometrical information relating each point to its neighbors, it does not directly allow computations involving



the large-scale structure of the graph. A convenient way to achieve this is by “integrating” the local distances into a partition tree.

Let  $X = \{x_1, \dots, x_n\}$  be a finite set. Consider a sequence of  $L$  finer and finer partitions of  $X$ , denoted  $\mathcal{V}^1, \dots, \mathcal{V}^L$ . For each  $1 \leq \ell \leq L$ , the partition at level  $\ell$  is composed of  $n(\ell)$  mutually disjoint sets, which we call folders,

$$\mathcal{V}^\ell = \{X_1^\ell, \dots, X_{n(\ell)}^\ell\} \quad (64)$$

such that

$$X = \biguplus_{k=1}^{n(\ell)} X_k^\ell. \quad (65)$$

The finest partition, at level  $\ell = L$ , is composed of  $n(L) = n$  singleton folders:  $X_k^L = \{x_k\}$  for  $k = 1, \dots, n$ . The coarsest partition, at level  $\ell = 1$ , is composed of a single folder,  $X_1^1 = X$ . The partitions are nested in the sense that for  $1 < \ell \leq L$ , each folder  $X_k^\ell \in \mathcal{V}^\ell$  is a subset of a folder from  $\mathcal{V}^{\ell-1}$ . We let  $\text{subfolders}(\ell, k) \subset \{1, \dots, n(\ell+1)\}$  be the indices such that

$$X_k^\ell = \biguplus_{j \in \text{subfolders}(\ell, k)} X_j^{\ell+1}. \quad (66)$$

### B.3 The Coupled Geometry of Questionnaires

In this section, we review the framework of coupled geometry introduced in [14, 25], which provides a multiscale approach to uncover the underlying structure of a matrix by simultaneously organizing its rows and columns. We begin with definitions of multiscale affinities.

**Definition B.1** (Mutiscale Tree Affinities). *Let  $X = \{x_1, \dots, x_N\}$  be a dataset, and let  $\mathcal{T}_X = \{\mathcal{V}^\ell\}$  denote a multiscale partition tree over  $X$  as defined in the previous section. For any function  $f : X \rightarrow \mathbb{R}$ , define the sample vector over folder  $X_k^\ell \in \mathcal{V}^\ell$  as*

$$f(X_k^\ell) := [f(x)]_{x \in X_k^\ell}. \quad (67)$$

*Let the weight function  $\omega : \mathcal{T}_X \rightarrow \mathbb{R}$  be given by*

$$\omega(X_k^\ell) := 2^{-a\ell} \cdot |X_k^\ell|^b, \quad (68)$$

*where  $a \in \mathbb{R}$  controls level sensitivity, and  $b \in \mathbb{R}$  modulates the influence of folder size. Given two functions  $f, g : X \rightarrow \mathbb{R}$ , the multiscale tree affinity*

over  $\mathcal{T}_X$  is defined as

$$D_{\mathcal{T}_X}(f, g) := \sum_{\mathcal{V}^\ell \in \mathcal{T}_X} \sum_{X_k^\ell \in \mathcal{V}^\ell} \left\| f(X_k^\ell) - g(X_k^\ell) \right\| \cdot \frac{\omega(X_k^\ell)}{|X_k^\ell|}. \quad (69)$$

The corresponding tree affinity is

$$W_{\mathcal{T}_X}(f, g) := \exp \left( -\frac{D_{\mathcal{T}_X}(f, g)}{\epsilon} \right), \quad (70)$$

where  $\epsilon > 0$  is a scaling parameter.

*Remark B.2.* In [16], several metrics as in (69) are defined and proved equivalent to Earth mover's distance (EMD) with respect to the tree metric. The parameters  $a$ ,  $b$ , and  $\epsilon$  modulate the effect of tree structure on the EMD. Increasing  $a$  places more weight on differences at coarser scales near the root, while  $a = 0$  yields uniform weighting across levels and  $a < 0$  emphasizes finer, leaf-level structure. The parameter  $b$  controls sensitivity to folder size:  $b > 0$  favors larger folders, while  $b < 0$  emphasizes smaller ones. The parameter  $\epsilon$  regulates the decay of the affinity; in practice, it is typically set as a constant multiple of the median EMD across all function pairs.

Now consider a matrix  $\mathcal{S} : Y \times X \rightarrow \mathbb{R}$ . We introduce the coupled geometry of rows and columns:

**Definition B.3** (Coupled Geometry). *Given a partition tree  $\mathcal{T}_X$  on  $X$ , the dual affinity between rows  $y_1, y_2 \in Y$  is defined as*

$$W_{\mathcal{T}_X}(y_1, y_2) := W_{\mathcal{T}_X}(S_{y_1}, S_{y_2}), \quad (71)$$

where each  $S_y(x) := S(y, x)$  is viewed as a function on  $X$ .

Similarly, given a partition tree  $\mathcal{T}_Y$  on  $Y$ , the dual affinity between columns  $x_1, x_2 \in X$  is defined as

$$W_{\mathcal{T}_Y}(x_1, x_2) := W_{\mathcal{T}_Y}(S^{x_1}, S^{x_2}), \quad (72)$$

where  $S^x(y) := S(y, x)$  is viewed as a function on  $Y$ .

Using these constructions, the Questionnaire algorithm [4] that iteratively refines the multiscale structures of rows and columns and the coupled geometry is:

---

**Algorithm 2** Questionnaire

---

1. Given initial affinity  $W_X$  on  $X$ , construct a tree  $\mathcal{T}_X$ .
  2. Compute the dual affinity  $W_{\mathcal{T}_X}$  on  $Y$  and build a tree  $\mathcal{T}_Y$ .
  3. Compute the dual affinity  $W_{\mathcal{T}_Y}$  on  $X$  and refine  $\mathcal{T}_X$ .
  4. Repeat steps 2 and 3 until either the affinities  $W_{\mathcal{T}_X}$  and  $W_{\mathcal{T}_Y}$  converge, or a fixed number of iterations is reached.
- 

In this work, the initial affinity matrix  $W_X$  is computed using a Gaussian kernel,  $W_X(i, j) = \exp\left(-\frac{\|x_i - x_j\|^2}{2\sigma^2}\right)$ , where  $\sigma = \text{median}_{x_i, x_j \in X} \|x_i - x_j\|_2$ . At each iteration, the construction and refinement of the tree  $\mathcal{T}_X$  (or  $\mathcal{T}_Y$ ) is performed via recursive spectral bipartitioning using the Fiedler vector associated with the affinity matrix  $W_{\mathcal{T}_X}$  (or  $W_{\mathcal{T}_Y}$ ). This yields a hierarchical organization that reflects the intrinsic geometry of the data. Through the iterative procedure in which the geometry of one dimension is refined based on the current organization of the other, we have an adaptive matrix reordering that reveals latent hierarchical patterns. These ideas are further developed in [4], which presents a practical implementation and experimental validation of the coupled geometry framework [3].

## C Walsh Wavelet Packet and Best Basis Selection

This section reviews key ideas from the work of Thiele and Villemoes [45], which introduced a fast, adaptive framework for time–frequency analysis based on Walsh tilings.

**Walsh Wavelet Packets.** The Walsh system  $\{W_n\}_{n=0}^\infty$  forms a complete orthonormal basis for  $L^2[0, 1)$ , consisting of piecewise constant functions that take values in  $\{\pm 1\}$ . These functions are defined recursively by

$$\begin{aligned} W_0(t) &= 1, \\ W_{2n}(t) &= W_n(2t) + (-1)^n W_n(2t - 1), \\ W_{2n+1}(t) &= W_n(2t) - (-1)^n W_n(2t - 1), \end{aligned} \tag{73}$$

for  $t \in [0, 1)$ , where each  $W_n$  has exactly  $n$  sign changes. A *tile* is a dyadic rectangle of area one, parametrized by scale indices  $j, j', k, n \in \mathbb{N} \cup \{0\}$ , with  $k < 2^j$ . The associated time interval and frequency band are given by

$$I := [2^{-j}k, 2^{-j}(k+1)), \quad \omega := [2^{j'}n, 2^{j'}(n+1)). \tag{74}$$

When  $j = j'$ , the tile  $p = I \times \omega$  is considered unit-area. Let  $\mathcal{P}$  be the collection of all of these unit-area dyadic rectangles. A localized Walsh function associated with tile  $\mathbf{p} \in \mathcal{P}$  is then defined as

$$w_{\mathbf{p}}(t) = w_{j,k,n}(t) := 2^{j/2} W_n(2^j t - k), \quad (75)$$

which is supported on  $I$  and has  $n$  sign changes corresponding to the frequency band  $\omega$ .

Let  $N = 2^L$  denote the signal length. A discrete signal of length  $N$  can be viewed as a piecewise constant function  $f: [0, N) \rightarrow \mathbb{R}$ , where the function is constant on each unit interval  $[n, n+1)$ , for  $n = 0, 1, \dots, N-1$ . The Walsh wavelet packet framework constructs an overcomplete dictionary of orthonormal functions by associating each basis atom  $w_p$  with a dyadic space-frequency tile  $p \subset \mathcal{S}_N := [0, N) \times [0, 1)$ . At each scale  $j = 0, 1, \dots, L$ , the domain  $\mathcal{S}_N$  is partitioned into  $N$  disjoint tiles, yielding a total of  $(L+1)N$  candidate atoms. Any orthonormal basis corresponds to an admissible tiling  $\mathcal{B} \subset \mathcal{P}$ , where  $\mathcal{P}$  denotes the full collection of tiles. The signal admits the expansion

$$f(x) = \sum_{\mathbf{p} \in \mathcal{B}} \langle f, w_{\mathbf{p}} \rangle w_{\mathbf{p}}(x), \quad (76)$$

where orthogonality holds whenever the tiles are disjoint, i.e.,  $\mathbf{p} \cap \tilde{\mathbf{p}} = \emptyset$  for all  $\mathbf{p} \neq \tilde{\mathbf{p}} \in \mathcal{B}$ . The Walsh transform coefficients  $\langle f, w_p \rangle$  can be computed efficiently in  $O(N \log N)$  time using the Fast Walsh–Hadamard Transform (FWHT) [24], which leverages the binary structure of the basis and requires only additions and subtractions.

This construction extends naturally to two-dimensional signals. Let  $S: [0, N_Y) \times [0, N_X) \rightarrow \mathbb{R}$  denote an image of size  $N_Y \times N_X$ , where  $N_X = 2^L$  and  $N_Y = 2^{L'}$ . The two-dimensional Walsh wavelet packet dictionary is formed via tensor products of one-dimensional atoms:

$$w_{(\mathbf{p}, \mathbf{q})}(x, y) := w_{\mathbf{p}}(x) w_{\mathbf{q}}(y), \quad (\mathbf{p}, \mathbf{q}) \in \mathcal{P}_X \times \mathcal{P}_Y, \quad (77)$$

where each index  $(\mathbf{p}, \mathbf{q})$  corresponds to a dyadic tile in the product domain  $\mathcal{S}_{N_Y} \times \mathcal{S}_{N_X}$ . The total number of atoms in this dictionary is  $(L' + 1)N_Y \times (L + 1)N_X$ , and any admissible two-dimensional basis corresponds to a tiling  $\mathcal{B} \subset \mathcal{P}_Y \times \mathcal{P}_X$ . The image may be represented as

$$S(x, y) = \sum_{(\mathbf{p}, \mathbf{q}) \in \mathcal{B}} \langle S, w_{(\mathbf{p}, \mathbf{q})} \rangle w_{(\mathbf{p}, \mathbf{q})}(x, y), \quad (78)$$

with orthogonality satisfied whenever  $\mathbf{p} \cap \tilde{\mathbf{p}} = \emptyset$  or  $\mathbf{q} \cap \tilde{\mathbf{q}} = \emptyset$  for all  $(\mathbf{p}, \mathbf{q}), (\tilde{\mathbf{p}}, \tilde{\mathbf{q}}) \in \mathcal{B}$ .

**Best Basis Selection.** Given a signal  $f$  of length  $N = 2^L$ , the objective of the best basis selection is to select a tiling  $\mathcal{B} \subset \mathcal{P}$  such that the associated basis  $\{w_{\mathbf{p}}\}_{\mathbf{p} \in \mathcal{B}}$  yields an efficient representation of  $f$ . A cost function  $c(\mathbf{p})$  is assigned to each tile  $\mathbf{p} \in \mathcal{P}$ , typically defined in terms of the magnitude of the transform coefficient  $\langle f, w_{\mathbf{p}} \rangle$ . A common choice is

$$c(\mathbf{p}) := |\langle f, w_{\mathbf{p}} \rangle|^\ell, \quad (79)$$

for  $0 < \ell < 2$ . The total cost over a tiling  $\mathcal{B}$  of  $\mathcal{S}_N$  is then given by

$$C(f, \mathcal{B}) := \sum_{\mathbf{p} \in \mathcal{B}} c(\mathbf{p}). \quad (80)$$

This cost functional is designed to be small when the energy of  $f$  is concentrated in a small number of significant coefficients  $\langle f, w_{\mathbf{p}} \rangle$ , making it well suited for selecting sparse or compact representations.

The *best basis* is the tiling  $\mathcal{B}^* = \arg \min_{\mathcal{B}} C(f, \mathcal{B})$ , that minimizes the total cost  $C(f, \mathcal{B})$  over all admissible tilings of  $\mathcal{S}_N$ . Thiele and Villemonais [45] proposed a dynamic programming algorithm that compares the cost of a parent tile with the combined cost of its horizontal and vertical splits, and selects the configuration with the lower total cost. This recursive process efficiently identifies the optimal decomposition. For a signal with length  $N$ , the total computational complexity of the method is of  $O(N \log N)$ .

This one-dimensional framework was later extended to two-dimensional signals, particularly in the context of image compression [34]. In the 2D setting, the analysis domain becomes  $S(x, y)$  on  $[0, N_X) \times [0, N_Y)$ , and adaptive tilings are constructed over dyadic rectangles in the joint space–frequency plane  $\mathcal{S}_{N_X} \times \mathcal{S}_{N_Y}$ . Each 2D tile corresponds to a separable product of 1D tiles. The best-basis selection algorithm applies analogously in two dimensions, recursively minimizing the total cost across hierarchical tilings. The total computational complexity is of  $O(N_X N_Y (\log N_X \log N_Y))$ . We suggest that readers refer to [45, 34] for the technical details.

**Extension to General Graph Domains.** The Generalized Haar-Walsh Transform (GHWT) [29, 39] extends the classical Haar-Walsh wavelet packet framework to signals supported on general graphs. It constructs a hierarchical dictionary of orthonormal basis vectors by recursively applying localized averaging and differencing operations over a tree-structured partition of the vertex set. Unlike classical wavelet packets, which operate on uniformly spaced dyadic intervals with an inherent linear ordering, the GHWT

accommodates domains without a global coordinate system. The underlying partition tree is not restricted to binary splits; nodes may be divided into arbitrary subsets, enabling adaptive tilings that reflect the geometry of the underlying graph, while still permitting coefficient computation with  $O(N \log N)$  complexity, analogous to the FWHT.

The extended GHWT (eGHWT) [39] further enhances this framework by implementing a best-basis selection algorithm over the GHWT dictionary, analogous to the one- and two-dimensional best-basis algorithms developed for Haar-Walsh wavelet packets. This allows for the adaptive selection of an orthonormal basis that minimizes a user-defined cost functional, such as entropy or sparsity. The algorithm is applicable to signals of arbitrary length on graphs of general structure, without requiring  $N = 2^L$ . The overall computational complexity is  $O(N \log N)$  for one-dimensional signals or graph-supported data under unbalanced hierarchical partitions. For two-dimensional signals, the complexity becomes  $O(N_X N_Y (\log N_X \log N_Y))$ , analogous to the classical 2D setting. We refer the reader to [29, 39] for algorithmic details.

## References

- [1] Sankaraleengam Alagapan, Hae Won Shin, Flavio Fröhlich, and Hau-Tieng Wu. Diffusion geometry approach to efficiently remove electrical stimulation artifacts in intracranial electroencephalography. *Journal of neural engineering*, 16(3):036010, 2019.
- [2] Jerrod Ankenman and William Leeb. Mixed hölder matrix discovery via wavelet shrinkage and calderón–zygmund decompositions. *Applied and Computational Harmonic Analysis*, 45(3):551–596, 2018.
- [3] Jerrod I. Ankenman. pyquest github repository. <https://github.com/hgfalling/pyquest>. Accessed: 2025-04-04.
- [4] Jerrod Isaac Ankenman. *Geometry and analysis of dual networks on questionnaires*. Yale University, 2014.
- [5] Rasoul Anvari, Mokhtar Mohammadi, and Amin Roshandel Kahoo. Enhancing 3-d seismic data using the t-svd and optimal shrinkage of singular value. *IEEE Journal of Selected Topics in Applied Earth Observations and Remote Sensing*, 12(1):382–388, 2018.

- [6] Zhidong Bai and Jian-feng Yao. Central limit theorems for eigenvalues in a spiked population model. *Annales de l'IHP Probabilités et statistiques*, 44(3):447–474, 2008.
- [7] Zhidong Bai and Jianfeng Yao. On sample eigenvalues in a generalized spiked population model. *J. Multivar. Anal.*, 106:167–177, 2012.
- [8] Jinho Baik and Jack W Silverstein. Eigenvalues of large sample covariance matrices of spiked population models. *J. Multivar. Anal.*, 97(6):1382–1408, 2006.
- [9] Florent Benaych-Georges, Alice Guionnet, and Mylène Maida. Fluctuations of the extreme eigenvalues of finite rank deformations of random matrices. *Electron. J. Probab.*, 16:1621–1662, 2011.
- [10] Florent Benaych-Georges and Raj Rao Nadakuditi. The singular values and vectors of low rank perturbations of large rectangular random matrices. *J. Multivar. Anal.*, 111:120 – 135, 2012.
- [11] Florent Benaych-Georges and Raj Rao Nadakuditi. The singular values and vectors of low rank perturbations of large rectangular random matrices. *Journal of Multivariate Analysis*, 111:120–135, 2012.
- [12] Ralf Bousseljot, Dieter Kreiseler, and Allard Schnabel. Nutzung der ekg-signaldatenbank cardiodat der ptb über das internet. 1995.
- [13] Neng-Tai Chiu, Stephanie Huwiler, M Laura Ferster, Walter Karlen, Hau-Tieng Wu, and Caroline Lustenberger. Get rid of the beat in mobile eeg applications: A framework towards automated cardiogenic artifact detection and removal in single-channel eeg. *Biomed Signal Process Control*, 72:103220, 2022.
- [14] Ronald R Coifman and Matan Gavish. Harmonic analysis of digital data bases. *Wavelets and Multiscale Analysis: Theory and Applications*, pages 161–197, 2011.
- [15] Ronald R Coifman and Stéphane Lafon. Diffusion maps. *Applied and computational harmonic analysis*, 21(1):5–30, 2006.
- [16] Ronald R Coifman and WE Leeb. Earth mover’s distance and equivalent metrics for spaces with hierarchical partition trees. *Yale CS Technical Report*, 2013.

- [17] Xiukai Ding and Fan Yang. Spiked separable covariance matrices and principal components. *The Annals of Statistics*, 49(2):1113 – 1138, 2021.
- [18] David L Donoho, Matan Gavish, and Iain M Johnstone. Optimal shrinkage of eigenvalues in the spiked covariance model. *Ann. Stat.*, 46(4):1742, 2018.
- [19] David L Donoho, Matan Gavish, and Elad Romanov. ScreeNOT: Exact mse-optimal singular value thresholding in correlated noise. *arXiv preprint arXiv:2009.12297*, 2020.
- [20] David L Donoho and Iain M Johnstone. Ideal spatial adaptation by wavelet shrinkage. *biometrika*, 81(3):425–455, 1994.
- [21] David L Donoho and Iain M Johnstone. Adapting to unknown smoothness via wavelet shrinkage. *Journal of the american statistical association*, 90(432):1200–1224, 1995.
- [22] David L Donoho and Iain M Johnstone. Neo-classical minimax problems, thresholding and adaptive function estimation. *Bernoulli*, 2(1):39–62, 1996.
- [23] Carl Eckart and Gale Young. The approximation of one matrix by another of lower rank. *Psychometrika*, 1(3):211–218, 1936.
- [24] Fino and Algazi. Unified matrix treatment of the fast walsh-hadamard transform. *IEEE Transactions on Computers*, 100(11):1142–1146, 1976.
- [25] Matan Gavish and Ronald R Coifman. Sampling, denoising and compression of matrices by coherent matrix organization. *Applied and Computational Harmonic Analysis*, 33(3):354–369, 2012.
- [26] Matan Gavish and David L. Donoho. Optimal shrinkage of singular values. *IEEE Trans. Inform. Theory*, 63(4):2137–2152, 2017.
- [27] Matan Gavish, Boaz Nadler, and Ronald R Coifman. Multiscale wavelets on trees, graphs and high dimensional data: theory and applications to semi supervised learning. In *ICML*, volume 10, pages 367–74, 2010.
- [28] Gene Golub and William Kahan. Calculating the singular values and pseudo-inverse of a matrix. *Journal of the Society for Industrial and Applied Mathematics, Series B: Numerical Analysis*, 2(2):205–224, 1965.



- [29] Jeff Irion and Naoki Saito. Applied and computational harmonic analysis on graphs and networks. In *Wavelets and Sparsity XVI*, volume 9597, pages 336–350. SPIE, 2015.
- [30] William Leeb. Rapid evaluation of the spectral signal detection threshold and stieltjes transform. *Advances in Computational Mathematics*, 47(4):1–29, 2021.
- [31] William Leeb. Optimal singular value shrinkage for operator norm loss: Extending to non-square matrices. *Statistics & Probability Letters*, 186:109472, 2022.
- [32] William Leeb and Elad Romanov. Optimal spectral shrinkage and pca with heteroscedastic noise. *IEEE Trans. Inform. Theory*, 67(5):3009–3037, 2021.
- [33] William E Leeb. Matrix denoising for weighted loss functions and heterogeneous signals. *SIAM Journal on Mathematics of Data Science*, 3(3):987–1012, 2021.
- [34] Maj Lindberg and Lars F Villemoes. Image compression with adaptive haar-walsh tilings. In *Wavelet Applications in Signal and Image Processing VIII*, volume 4119, pages 911–921. SPIE, 2000.
- [35] Jun Liu, Xiangqian Liu, and Xiaoli Ma. First-order perturbation analysis of singular vectors in singular value decomposition. *IEEE Transactions on Signal Processing*, 56(7):3044–3049, 2008.
- [36] Tzu-Chi Liu, Yi-Wen Liu, and Hau-Tieng Wu. Denoising click-evoked otoacoustic emission signals by optimal shrinkage. *J. Acoust. Soc. Am.*, 149(4):2659–2670, 2021.
- [37] Leon Mirsky. Symmetric gauge functions and unitarily invariant norms. *The quarterly journal of mathematics*, 11(1):50–59, 1960.
- [38] Raj Rao Nadakuditi. Optshrink: An algorithm for improved low-rank signal matrix denoising by optimal, data-driven singular value shrinkage. *IEEE Transactions on Information Theory*, 60(5):3002–3018, 2014.
- [39] Naoki Saito and Yiqun Shao. eGHWT: The extended generalized Haar-Walsh transform. *J. Math. Imaging Vis.*, 64(3):261–283, 2022.
- [40] Andrey A Shabalin and Andrew B Nobel. Reconstruction of a low-rank matrix in the presence of gaussian noise. *J. Multivar. Anal.*, 118:67–76, 2013.

- [41] Pei-Chun Su and Ronald R Coifman. Learning the analytic geometry of transformations to achieve efficient computation. *arXiv preprint arXiv:2506.11990*, 2025.
- [42] Pei-Chun Su, Stephen Miller, Salim Idriss, Piers Barker, and Hau-Tieng Wu. Recovery of the fetal electrocardiogram for morphological analysis from two trans-abdominal channels via optimal shrinkage. *Physiol. Meas.*, 40(11):115005, 2019.
- [43] Pei-Chun Su, Elsayed Z Soliman, and Hau-Tieng Wu. Robust t-end detection via t-end signal quality index and optimal shrinkage. *Sensors*, 20(24):7052, 2020.
- [44] Pei-Chun Su and Hau-Tieng Wu. Data-driven optimal shrinkage of singular values under high-dimensional noise with separable covariance structure. *arXiv preprint arXiv:2207.03466*, 2022.
- [45] Christoph M Thiele and Lars F Villemoes. A fast algorithm for adapted time–frequency tilings. *Applied and Computational Harmonic Analysis*, 3(2):91–99, 1996.
- [46] Jelle Veraart, Dmitry S Novikov, Daan Christiaens, Benjamin Ades-Aron, Jan Sijbers, and Els Fieremans. Denoising of diffusion mri using random matrix theory. *Neuroimage*, 142:394–406, 2016.
- [47] Roman Vershynin. *High-dimensional probability: An introduction with applications in data science*, volume 47. Cambridge university press, 2018.